

Higgs boson to γZ decay as a probe of flavour changing neutral Yukawa couplings

Shi-Ping He^{1,*}

¹*Center for Future High Energy Physics and Theoretical Physics Division,
Institute of High Energy Physics, Chinese Academy of Sciences, Beijing 100049, China*

(Dated: March 14, 2024)

With the deeper study of Higgs particle, Higgs precision measurements can be served to probe new physics indirectly. In many new physics models, vector-like quarks T_L, T_R occur naturally. It is important to probe their couplings with standard model particles. In this work, we consider the singlet T_L, T_R extended models and show how to constrain the Tth couplings through the $h \rightarrow \gamma Z$ decay at high-luminosity LHC. Firstly, we derive the perturbative unitarity bounds on $|y_{L,R}^{tT}|$ with other couplings set to be zeros simply. To optimize the situation, we take $m_T = 400$ GeV and $s_L = 0.2$ considering the experimental constraints. Under this benchmark point, we find that the future bounds from $h \rightarrow \gamma Z$ decay can limit the real parts of $y_{L,R}^{tT}$ in the positive direction to be $O(1)$ because of the double enhancement. For the real parts of $y_{L,R}^{tT}$ in the negative direction, it is always surpassed by the perturbative unitarity. Moreover, we find that the top quark electric dipole moment can give stronger bounds (especially the imaginary parts of $y_{L,R}^{tT}$) than the perturbative unitarity and $h \rightarrow \gamma Z$ decay in the off-axis regions for some scenarios.

* sphe@ihep.ac.cn

I. INTRODUCTION

The standard model (SM) of elementary particle physics was proposed in the 1960s [1], and it has been verified to be quite successful up to now. However, there are still many problems beyond the ability of SM, for example, Higgs mass naturalness, gauge coupling unification, fermion mass hierarchy, electro-weak vacuum stability, dark matter, matter anti-matter asymmetry, and so on. Thus, new physics beyond the SM (BSM) are motivated in the high energy physics community. Many of these BSM models predict the existence of heavy fermions, for example, composite Higgs models [2, 3], little Higgs models [4, 5], grand unified theories [6], extra dimension models [7]. In these models, there can be a heavy up-type quark T , which interacts with the SM particles through TbW, TtZ, Tth interactions. Analyses on these couplings may tell us some clues about the new physics. TbW coupling can be constrained from single production of T quark, but there are always many assumptions for most of the current constraints. It will be hard for the detection of the flavour changing neutral (FCN) couplings TtZ, Tth , because T productions from tZ, th fusion are highly suppressed. If there exist other new decay channels for the T quark¹, even the bounded TbW coupling can be saturated. Since the discovery of Higgs boson at the Large Hadron Collider (LHC) [8], it can also be a probe to such new physics.

Currently, all the main production and decay channels of the Higgs boson have been discovered at the LHC. Then, the next step is to measure the observed channels more accurately. At the same time, attention should be paid to the undiscovered channels. Precision measurements of the Higgs particle may help us decipher the nature of electro-weak symmetry breaking (EWSB) [9] and open the door to new physics [10]. hVV and hff couplings inferred from the observed channels are SM-like now, while there can still be large deviations for the rare decay modes, for example, $h \rightarrow \gamma Z, \mu^+ \mu^-$. The γZ decay mode has drawn much attention of this community. It can be used to detect CP violation [11–13] and many new physics scenarios [14–16]. Here, we will show how to constrain the FCN Yukawa (FCNY) couplings through the $h \rightarrow \gamma Z$ decay mode indirectly. The constraints from $h \rightarrow \gamma Z$ do not depend on the total width of T quark, namely, in spite of other decay modes.

In this paper, we build the framework of FCN couplings in Sec. II firstly. Sec. III is devoted to the theoretical and experimental constraints on the simplified model. In Sec. IV, we compute the new physics contributions to the partial decay width of $h \rightarrow \gamma Z$. Then, we perform the numerical constraints on the FCNY interactions in Sec. V. Finally, we give the summary and conclusions in Sec. VI.

II. FRAMEWORK OF FLAVOUR CHANGING NEUTRAL COUPLINGS

II.1. UV complete model

It is strongly constrained for the mixings between heavy particles and the first two generations because of the bounds from flavour physics [17–19]. What is more, the third generation is more likely to be concerned with new physics theoretically owing to the mass hierarchy. For convenience and simplicity, we only take into account the mixings between the third generation and heavy quarks.

¹ Say $T \rightarrow tS$, here S can be a CP even or odd new scalar.

Based on the SM gauge group $SU_C(3) \otimes SU_L(2) \otimes U_Y(1)$, we can enlarge the SM by adding new particles with different representations. Usually, we extend the SM fermion sector by introducing vector-like particles to avoid the quantum anomaly. The minimal extension of quark sector is to add one pair of vector-like quarks (VLQs) [20, 21]. For the non-minimally extended models, the scalar sector can also be augmented. Besides the VLQs, we can also plus a real gauge singlet scalar [22–24], a Higgs doublet [25], and even both the singlet-doublet scalars at the same time [25, 26]. In these models, there can exist other decay channels [27, 28].

FCN couplings TtZ and Tth show different patterns in different models. For simplicity, we will only consider the case where there is one pair of VLQs T_L and T_R .² In the following, we will give two specific examples: the minimal extension with a pair of singlet quarks T_L, T_R (gauge group representation $(3, 0, 2/3)$) and the model further enlarged by an extra real singlet scalar (gauge group representation $(1, 0, 0)$).

II.1.1. Minimal vector-like quark model

Let us start with the model by adding a pair of singlet fermions T_L, T_R to the SM, which is dubbed as the VLQT model. The Lagrangian can be written as [21]

$$\begin{aligned} \mathcal{L} &= \mathcal{L}_{SM} + \mathcal{L}_T^{Yukawa} + \mathcal{L}_T^{gauge}, \\ \mathcal{L}_T^{Yukawa} &= -\Gamma_T^i \bar{Q}_L^i \tilde{\Phi} T_R - M_T \bar{T}_L T_R + \text{h.c.}, \quad \mathcal{L}_T^{gauge} = \bar{T}_L i \not{D} T_L + \bar{T}_R i \not{D} T_R, \end{aligned} \quad (1)$$

where $\tilde{\Phi} = i\sigma_2 \Phi^*$ and the covariant derivative is defined as $D_\mu = \partial_\mu - ig' Y_T B_\mu$. Y_T and Q_T are the $U_Y(1)$ and electric charge of the T quark, respectively. The Higgs doublet is parametrized as $\Phi^T = [\phi^+, \frac{v+h+i\chi}{\sqrt{2}}]$.

It is easy to obtain the mass terms of t and T quarks³:

$$\mathcal{L}_{mass} \supset - \begin{bmatrix} \bar{t}_L & \bar{T}_L \end{bmatrix} \begin{bmatrix} \frac{1}{\sqrt{2}} \Gamma_t^{33} v & \frac{1}{\sqrt{2}} \Gamma_T^{33} v \\ 0 & M_T \end{bmatrix} \begin{bmatrix} t_R \\ T_R \end{bmatrix} + \text{h.c.} \quad (2)$$

Here, Γ_t^{33} and Γ_T^{33} are the gauge eigenstate Yukawa couplings in front of $\bar{Q}_L^3 \tilde{\Phi} T_R$ and $\bar{Q}_L^3 \tilde{\Phi} t_R$ individually. The t and T quarks can be rotated into mass eigenstates by the following transformations:

$$\begin{bmatrix} t_L \\ T_L \end{bmatrix} \rightarrow \begin{bmatrix} \cos \theta_L & \sin \theta_L \\ -\sin \theta_L & \cos \theta_L \end{bmatrix} \begin{bmatrix} t_L \\ T_L \end{bmatrix}, \quad \begin{bmatrix} t_R \\ T_R \end{bmatrix} \rightarrow \begin{bmatrix} \cos \theta_R & \sin \theta_R \\ -\sin \theta_R & \cos \theta_R \end{bmatrix} \begin{bmatrix} t_R \\ T_R \end{bmatrix}. \quad (3)$$

Then, we have the following mass eigenstate Yukawa interactions:

$$\begin{aligned} \mathcal{L}_{Yukawa} &\supset -m_t \bar{t} t - m_T \bar{T} T - \frac{m_t}{v} c_L^2 h \bar{t} t - \frac{m_T}{v} s_L^2 h \bar{T} T \\ &\quad - \frac{m_T}{v} s_L c_L h (\bar{t}_L T_R + \bar{T}_R t_L) - \frac{m_t}{v} s_L c_L h (\bar{T}_L t_R + \bar{t}_R T_L). \end{aligned} \quad (4)$$

² Of course, one can build one model with more T_L, T_R quarks. But the mass matrix may be equal to and even greater than three dimensions, which are quite complex.

³ Although the mass mixing term $\bar{T}_L t_R$ can appear, it will be removed via field redefinition [29, 30].

Here, s_L, c_L, s_R, c_R are short for $\sin \theta_L, \cos \theta_L, \sin \theta_R, \cos \theta_R$, respectively. Similarly, we abbreviate $\sin \theta, \cos \theta$ as s_θ, c_θ in the following context. In this model, we have two independent extra parameters m_T and θ_L . There are two relations between the mixing angles and t, T quark masses:

$$\tan \theta_R = \frac{m_t}{m_T} \tan \theta_L, \quad M_T^2 = m_T^2 c_L^2 + m_t^2 s_L^2. \quad (5)$$

For the singlet T_L and T_R quarks, the gauge eigenstate t, T quarks will interact with Z, W bosons through the following form:

$$\begin{aligned} \mathcal{L}_{gauge} \supset & \frac{g}{c_W} Z_\mu [\bar{t}_L \gamma^\mu (\frac{1}{2} - \frac{2}{3} s_W^2) t_L - \frac{2}{3} s_W^2 \bar{t}_R \gamma^\mu t_R - Q_T s_W^2 (\bar{T}_L \gamma^\mu T_L + \bar{T}_R \gamma^\mu T_R)] \\ & + \frac{g}{\sqrt{2}} (W_\mu^+ \bar{t}_L \gamma^\mu b_L + W_\mu^- \bar{b}_L \gamma^\mu t_L). \end{aligned} \quad (6)$$

Here, t and T quarks can be rotated into mass eigenstates by the transformations in Eq. (3). Thus, we have the following mass eigenstate gauge interactions:

$$\begin{aligned} \mathcal{L}_{gauge} \supset & \frac{g}{c_W} Z_\mu [(\frac{1}{2} c_L^2 - \frac{2}{3} s_W^2) \bar{t}_L \gamma^\mu t_L + (\frac{1}{2} s_L^2 - \frac{2}{3} s_W^2) \bar{T}_L \gamma^\mu T_L + \frac{1}{2} s_L c_L (\bar{t}_L \gamma^\mu T_L + \bar{T}_L \gamma^\mu t_L) \\ & - \frac{2}{3} s_W^2 \bar{t}_R \gamma^\mu t_R - \frac{2}{3} s_W^2 \bar{T}_R \gamma^\mu T_R] + \frac{g c_L}{\sqrt{2}} (W_\mu^+ \bar{t}_L \gamma^\mu b_L + W_\mu^- \bar{b}_L \gamma^\mu t_L) + \frac{g s_L}{\sqrt{2}} (W_\mu^+ \bar{T}_L \gamma^\mu b_L + W_\mu^- \bar{b}_L \gamma^\mu T_L). \end{aligned} \quad (7)$$

II.1.2. Vector-like quark and one singlet scalar model

Now, let us consider the model with SM extended by a pair of singlet VLQs T_L, T_R and a real singlet scalar S , which is named as VLQT+S. The Lagrangian can be written as [23, 31]

$$\begin{aligned} \mathcal{L} &= \mathcal{L}_{SM} + \mathcal{L}_T^{Yukawa} + \mathcal{L}_T^{gauge} + \mathcal{L}_S, \\ \mathcal{L}_T^{Yukawa} &= -\Gamma_T^i \bar{Q}_L^i \tilde{\Phi} T_R - M_T \bar{T}_L T_R - y_T^S S \bar{T}_L T_R + \text{h.c.}, \quad \mathcal{L}_T^{gauge} = \bar{T}_L i \not{D} T_L + \bar{T}_R i \not{D} T_R, \\ \mathcal{L}_S &= \frac{1}{2} \partial_\mu S \partial^\mu S - V_{\Phi S}, \quad V_{\Phi S} = \mu_{\Phi S} \Phi^\dagger \Phi S + \lambda_{\Phi S} \Phi^\dagger \Phi S^2 + t_S S + m_S^2 S^2 + \mu_S S^3 + \lambda_S S^4. \end{aligned} \quad (8)$$

Note that the Lagrangian form is invariant after shifting S ; thus, we can set $\langle S \rangle = 0$ through redefinition of the scalar field S [32–37]. Here, h can mix with S , so we should transform them into mass eigenstates via following rotations:

$$\begin{bmatrix} h \\ S \end{bmatrix} \rightarrow \begin{bmatrix} \cos \theta & \sin \theta \\ -\sin \theta & \cos \theta \end{bmatrix} \begin{bmatrix} h \\ S \end{bmatrix}. \quad (9)$$

The mass terms of t and T quarks are exactly the same as those in Eq. (2); thus, they can be rotated into mass eigenstates by the same transformations of Eq. (3). There is one extra Yukawa term $-y_T^S S \bar{T}_L T_R$ compared to the model VLQ, so the Yukawa interactions in this model are more

complex. Then we have the following mass eigenstate Yukawa interactions:

$$\begin{aligned}
\mathcal{L}_{Yukawa} \supset & -m_t \bar{t}t - m_T \bar{T}T - \left[\frac{m_t}{v} c_L^2 c_\theta - \text{Re}(y_T^S) s_L s_R s_\theta \right] h \bar{t}t - \left[\frac{m_T}{v} s_L^2 c_\theta - \text{Re}(y_T^S) c_L c_R s_\theta \right] h \bar{T}T \\
& - \left[\frac{m_T}{v} s_L c_L c_\theta + \text{Re}(y_T^S) s_L c_R s_\theta \right] h (\bar{t}_L T_R + \bar{T}_R t_L) - \left[\frac{m_t}{v} s_L c_L c_\theta + \text{Re}(y_T^S) c_L s_R s_\theta \right] h (\bar{T}_L t_R + \bar{t}_R T_L) \\
& + i \text{Im}(y_T^S) s_L s_R s_\theta h \bar{t} \gamma^5 t + i \text{Im}(y_T^S) c_L c_R s_\theta h \bar{T} \gamma^5 T \\
& - i \text{Im}(y_T^S) s_L c_R s_\theta h (\bar{t}_L T_R - \bar{T}_R t_L) - i \text{Im}(y_T^S) c_L s_R s_\theta h (\bar{T}_L t_R - \bar{t}_R T_L).
\end{aligned} \tag{10}$$

The gauge interactions for t and T quarks are fully the same as those in Eq. (6) and Eq. (7). In this model, there are four interesting parameters $\theta_L, m_T, \theta, y_T^S$. The other parameters in scalar potential do not have relation with the $h \rightarrow \gamma Z, \gamma\gamma$ processes.

II.2. Simplified model

Here, we will adopt one more general and model independent framework [38]. For simplicity, we only consider the singlet $T_{L,R}$ case. In the simplified model case, we can write down the related mass eigenstate state interactions generally:

$$\begin{aligned}
\mathcal{L} \supset & -m_t \bar{t}t - m_T \bar{T}T - e A_\mu \sum_{f=t,T} Q_f \bar{f} \gamma^\mu f + e Z_\mu [\bar{t} \gamma^\mu (g_L^t \omega_- + g_R^t \omega_+) t + \bar{T} \gamma^\mu (g_L^T \omega_- + g_R^T \omega_+) T \\
& + \bar{t} \gamma^\mu (g_L^{tT} \omega_- + g_R^{tT} \omega_+) T + \bar{T} \gamma^\mu (g_L^{tT} \omega_- + g_R^{tT} \omega_+) t] - \frac{m_t}{v} h \bar{t} (\kappa_t + i \gamma^5 \tilde{\kappa}_t) t + h \bar{T} (y_T + i \gamma^5 \tilde{y}_T) T \\
& + h \bar{t} (y_L^{tT} \omega_- + y_R^{tT} \omega_+) T + h \bar{T} ((y_L^{tT})^* \omega_+ + (y_R^{tT})^* \omega_-) t + \frac{g_{CL}}{\sqrt{2}} (W_\mu^+ \bar{t}_L \gamma^\mu b_L + W_\mu^- \bar{b}_L \gamma^\mu t_L) \\
& + \frac{g_{SL}}{\sqrt{2}} (W_\mu^+ \bar{T}_L \gamma^\mu b_L + W_\mu^- \bar{b}_L \gamma^\mu T_L),
\end{aligned} \tag{11}$$

where ω_\pm are the chirality projection operators $(1 \pm \gamma^5)/2$ and the gauge couplings are listed as follows:

$$\begin{aligned}
g_L^t &= \frac{1}{s_W c_W} \left(\frac{1}{2} c_L^2 - \frac{2}{3} s_W^2 \right), \quad g_L^T = \frac{1}{s_W c_W} \left(\frac{1}{2} s_L^2 - \frac{2}{3} s_W^2 \right), \quad g_L^{tT} = \frac{s_L c_L}{2 s_W c_W}, \\
g_R^t &= -\frac{2 s_W}{c_W}, \quad g_R^T = -\frac{2 s_W}{c_W}, \quad g_R^{tT} = 0.
\end{aligned} \tag{12}$$

Here, $m_T, \theta_L, \theta_R, \kappa_t, \tilde{\kappa}_t, y_T, \tilde{y}_T$ are all real parameters⁴, while y_L^{tT}, y_R^{tT} can be complex numbers. From now on, we will turn off the parameters $\tilde{\kappa}_t$ and \tilde{y}_T for simplicity.

In Tab. I, we give the expressions of $\kappa_t, y_T, y_L^{tT}, y_R^{tT}$ in three models. In Tab. II, we also give the expressions of $g_L^{tT} (y_L^{tT})^*, g_R^{tT} (y_R^{tT})^*, g_L^{tT} (y_R^{tT})^*, g_R^{tT} (y_L^{tT})^*$ in the VLQT and VLQT+S models. Here, we want to show the feasibility to constrain the FCNY couplings through the $h \rightarrow \gamma Z$ decay channel; thus, it is better to avoid drowning in elaborate theoretical calculations and collider phenomenology details. Although the FCNY couplings $y_{L,R}^{tT}$ are not free parameters in the mentioned VLQT and VLQT+S models, they can be free in more complex models because of enough degrees of freedom. For example, we can extend the SM by one pair of VLQs T_L, T_R and many real singlet scalars. Here, we want to make a general analysis naively, so we take them to be free.

⁴ Just as that we show in the above two models, θ_L, θ_R may be not independent rotation angles in specific models [21].

	SM	VLQT	VLQT+S
κ_t	1	c_L^2	$c_L^2 c_\theta - \frac{v s_L s_R s_\theta}{m_t} \text{Re}(y_T^S)$
y_T	\times	$-\frac{m_T}{v} s_L^2$	$-\frac{m_T}{v} s_L^2 c_\theta + \text{Re}(y_T^S) c_L c_R s_\theta$
$\text{Re}(y_L^{tT})$	\times	$-\frac{m_t}{v} s_L c_L$	$-\frac{m_t}{v} s_L c_L c_\theta - \text{Re}(y_T^S) c_L s_R s_\theta$
$\text{Re}(y_R^{tT})$	\times	$-\frac{m_T}{v} s_L c_L$	$-\frac{m_T}{v} s_L c_L c_\theta - \text{Re}(y_T^S) s_L c_R s_\theta$
$\text{Im}(y_L^{tT})$	\times	0	$\text{Im}(y_T^S) c_L s_R s_\theta$
$\text{Im}(y_R^{tT})$	\times	0	$-\text{Im}(y_T^S) s_L c_R s_\theta$

TABLE I. Patterns of Yukawa coefficients in SM, VLQT, and VLQT+S. There is no T quark in SM, so we use the symbol \times for T couplings.

	$g_L^{tT}(y_L^{tT})^*$	$g_R^{tT}(y_R^{tT})^*$	$g_L^{tT}(y_R^{tT})^*$	$g_R^{tT}(y_L^{tT})^*$
General	$\frac{1}{2s_W c_W} s_L c_L (y_L^{tT})^*$	0	$\frac{1}{2s_W c_W} s_L c_L (y_R^{tT})^*$	0
VLQT	$-\frac{m_t}{v} \frac{s_L^2 c_L^2}{2s_W c_W}$	0	$-\frac{m_T}{v} \frac{s_L^2 c_L^2}{2s_W c_W}$	0
VLQT+S	$\frac{s_L c_L^2}{2s_W c_W} (-\frac{m_t}{v} s_L c_\theta - y_T^S s_R s_\theta)$	0	$\frac{s_L^2 c_L}{2s_W c_W} [-\frac{m_T}{v} c_L c_\theta - (y_T^S)^* c_R s_\theta]$	0

TABLE II. Patterns of the multiplication of FCN couplings in VLQT and VLQT+S.

III. CONSTRAINTS ON THE MODEL

III.1. Perturbative unitarity bound

From theoretical point of view, large couplings may cause the problem of perturbative unitarity violation. One famous example is the upper limit of Higgs self-coupling (or the Higgs mass) in the SM [39]. For the scattering amplitude, we can perform the partial wave expansion: $M = 16\pi \sum_{l=0}^{\infty} (2l+1) a_l(s) P_l(\cos \theta)$. Then, the partial l -wave amplitude is $a_l(s) = \frac{1}{32\pi} \int_{-1}^1 d(\cos \theta) P_l(\cos \theta) M$. Especially, we have $a_0(s) = \frac{1}{32\pi} \int_{-1}^1 d(\cos \theta) M$, which should satisfy $|\text{Re}(a_0)| \leq \frac{1}{2}$. When you consider the two-to-two Higgs and longitudinally polarized vector boson scattering processes, S -wave unitarity will lead to the bound.

Similarly, we can bound the Yukawa couplings $y_{L,R}^{tT}$ from fermion scattering [40–43]. Then, we need to consider the two-to-two scattering processes with fermions. Obviously, there are two kinds of fermion processes: two-fermion and four-fermion processes. Actually, we only need to consider the neutral initial and final states. To simplify the analysis, we keep the y_L^{tT}, y_R^{tT} couplings but turn off the other couplings. After tedious computations, we get the following constraints (more details are given in App. A):

$$\sqrt{(|y_L^{tT}|^2 + |y_R^{tT}|^2)^2 + 12|y_L^{tT}|^2|y_R^{tT}|^2} + |y_L^{tT}|^2 + |y_R^{tT}|^2 \leq 16\pi. \quad (13)$$

In Fig. 1, we plot the parameter space region allowed by Eq. (13).

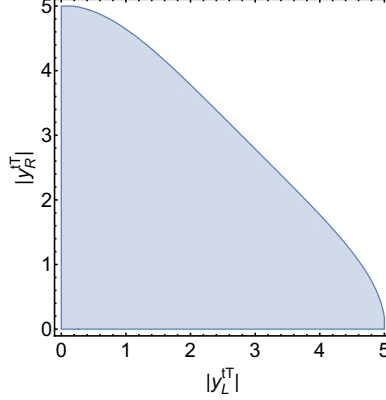


FIG. 1. The allowed region from perturbative unitarity in the plane of $|y_L^{tT}| - |y_R^{tT}|$.

III.2. Constraints from direct search

In the minimal extensions, the decay final states of T are bW^+ , tZ , th . According to the Goldstone boson equivalence theorem, the partial decay widths satisfy the identity $\Gamma(T \rightarrow tZ) \approx \Gamma(T \rightarrow th) \approx \frac{1}{2}\Gamma(T \rightarrow bW)$ approximately (or $Br(T \rightarrow tZ) \approx Br(T \rightarrow th) \approx 25\%$, $Br(T \rightarrow bW) \approx 50\%$). For the pair production of VLQs, the cross section is determined by the strong interaction. It will give us the model independent bound on the T quark mass, but we cannot get the information of T quark couplings. Assuming $Br(T \rightarrow tZ) + Br(T \rightarrow th) + Br(T \rightarrow bW) = 1$, the T quark mass below 700 GeV \sim TeV is excluded at 95% confidence level (CL) [44, 45]. The T quark can also be singly produced through TbW coupling. In the singlet T quark case, current constraints are $|s_L| \leq 0.2$ [46].

Current experiments give strong constraints on minimal VLQ models, but it will be relaxed in models with additional states. The mass can be light as 400 GeV if there exist an additional state mediated decay channels [28]. For the more complicated flavour and scalar sectors, there can be more than one mixing angle. The mixing angle is allowed to be larger.

III.3. Constraints from electro-weak precision measurements

The singlet VLQ T_L, T_R will contribute to the S, T parameters [47, 48]. The oblique corrections are mainly from the modification of SM gauge couplings and new particle loops. Their analytical expressions have been calculated in previous studies [19, 49, 50]:

$$\begin{aligned}
\Delta S &\equiv S - S^{SM} \\
&= -\frac{N_t^C s_L^2}{18\pi} [-2 \log r_{tT} + c_L^2 \frac{5 - 22r_{tT}^2 + 5r_{tT}^4}{(1 - r_{tT}^2)^2} + c_L^2 \frac{6(1 + r_{tT}^2)(1 - 4r_{tT}^2 + r_{tT}^4)}{(1 - r_{tT}^2)^3} \log r_{tT}], \\
\Delta T &\equiv T - T^{SM} = \frac{N_t^C m_t^2 s_L^2}{16\pi s_W^2 m_W^2} (-1 - c_L^2 + \frac{s_L^2}{r_{tT}^2} - \frac{4c_L^2}{1 - r_{tT}^2} \log r_{tT}),
\end{aligned} \tag{14}$$

with $r_{tT} \equiv \frac{m_t}{m_T}$. Now, let us define the $\Delta\chi^2$ as

$$\Delta\chi^2 \equiv \sum_{i,j=1,2} (O_i - O_i^{exp})(\sigma^2)_{ij}^{-1}(O_j - O_j^{exp}), \quad (15)$$

where $O_i \in \{\Delta S, \Delta T\}$, $(\sigma^2)_{ij} = \sigma_i \rho_{ij} \sigma_j$. Their values are listed as follows [51]:

$$\begin{aligned} \Delta S^{exp} &= 0.02, \quad \sigma_{\Delta S} = 0.07, \quad \Delta T^{exp} = 0.06, \quad \sigma_{\Delta T} = 0.06, \\ \rho &= \begin{bmatrix} 1 & 0.92 \\ 0.92 & 1 \end{bmatrix}, \quad \sigma^2 = \begin{bmatrix} \sigma_{\Delta S}^2 & 0 \\ 0 & \sigma_{\Delta T}^2 \end{bmatrix} \rho \begin{bmatrix} \sigma_{\Delta S}^2 & 0 \\ 0 & \sigma_{\Delta T}^2 \end{bmatrix}. \end{aligned} \quad (16)$$

In this paper, we choose the parameters to be $m_Z = 91.1876\text{GeV}$, $m_W = 80.387\text{GeV}$, $m_h =$

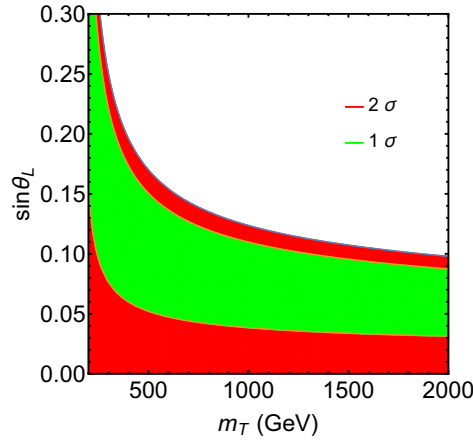


FIG. 2. The constraints on m_T, s_L from χ^2 -fit of the S, T parameters. Here the green and red areas are allowed at $1\sigma, 2\sigma$ CL, respectively.

125.09GeV , $m_t = 172.74\text{GeV}$, $G_F = 1.1664 \times 10^{-5}\text{GeV}^{-2}$, and $c_W = m_W/m_Z$ [51]. In Fig. 2, we get the constraints from the global fits of S, T parameters⁵.

III.4. Constraints from top physics

There are also constraints from the tbW anomalous coupling [52], which gives the bound $V_{tb} \geq 0.92$ at 95% CL assuming $V_{tb} \leq 1$ [53]. Then, we have $s_L \leq \sqrt{1 - V_{tb}} \approx 0.3$.

⁵ t - T mixing will also enter into $Zb\bar{b}$ coupling through one-loop correction, but here we will not consider them anymore.

III.5. Constraints from Higgs physics

In App. B, we give the exhaustive computations and analyses in both the SM and new physics model. When we take $\kappa_t = c_L^2$ and $y_T = -\frac{m_T}{v}s_L^2$ naively, the following expressions are obtained:

$$\begin{aligned}\mu_{\gamma\gamma} &\equiv \frac{\sigma(gg \rightarrow h)\Gamma(h \rightarrow \gamma\gamma)}{\sigma^{SM}(gg \rightarrow h)\Gamma^{SM}(h \rightarrow \gamma\gamma)} = \frac{\Gamma(h \rightarrow gg)\Gamma(h \rightarrow \gamma\gamma)}{\Gamma^{SM}(h \rightarrow gg)\Gamma^{SM}(h \rightarrow \gamma\gamma)} \\ &= |c_L^2 + s_L^2 \frac{F_f(\tau_T)}{F_f(\tau_t)}|^2 \frac{|N_t^C Q_t^2 [c_L^2 F_f(\tau_t) + s_L^2 F_f(\tau_T)] + F_W(\tau_W)|^2}{|N_t^C Q_t^2 F_f(\tau_t) + F_W(\tau_W)|^2}.\end{aligned}\quad (17)$$

In Fig. 3, we show the contour plot of $(\mu_{\gamma\gamma} - 1)$ in the parameter space of m_T, s_L . We find that the typical deviation $(\mu_{\gamma\gamma} - 1)$ is at the level of $-0.5\% \sim -5\%$, which is within the precision of current measurements [54]. As with the results in Ref. [50], the constraints from Higgs signal strength are quite loose.

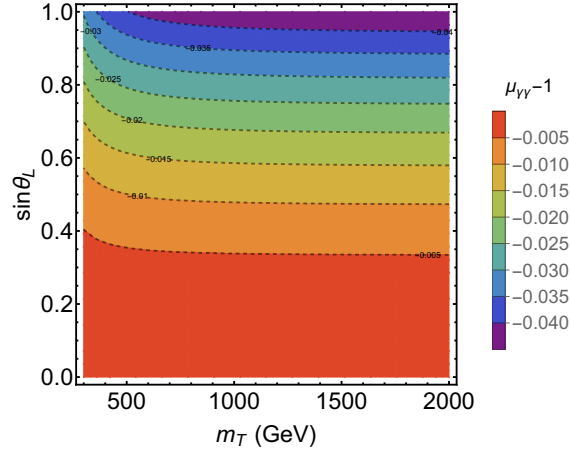


FIG. 3. The contour plot of the Higgs signal strength deviation for the $gg \rightarrow h \rightarrow \gamma\gamma$ channel in the $m_T - s_L$ plane.

III.6. Constraints from EDM

If there exist CP violation in the FCN interactions, it will contribute to the electron electric dipole moment (EDM). The neutron EDM and chromo EDM (CEDM) will also be affected. Then, the imaginary parts of $y_{L,R}^{iT}$ can be constrained. Here, CP violation is only from the FCNY interactions.

Firstly, the FCN couplings can alter the electron EDM through Barr-Zee diagrams at two-loop level [55] (see the left and middle diagrams of Fig. 4). Here, the contributions originate from the Z boson, because there are no FCN couplings for the photon. Due to the C invariance, only vectorial couplings can contribute [55]. Now, we can make a sketchy estimation. Compared to the photon diagram, Z boson mediated Barr-Zee diagrams are suppressed by $\lambda^2 \equiv \frac{g_L^{iT} + g_R^{iT}}{2Q_t} \frac{1 - 4s_W^2}{4s_W c_W} \sim 0.01$.

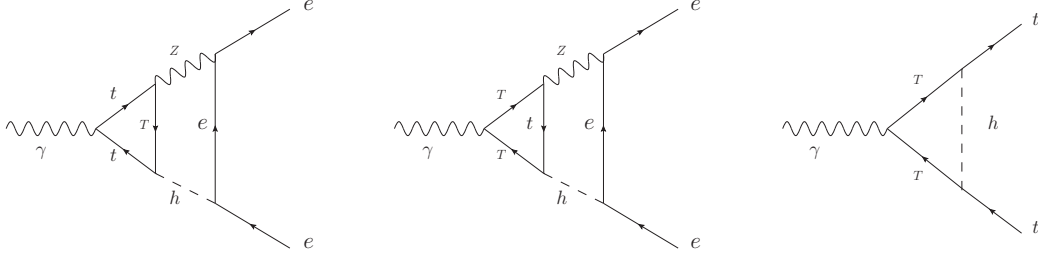


FIG. 4. The Barr-Zee diagrams contributing to the electron EDM (left, middle) and the Feynman diagrams contributing to the top quark EDM (right). For the fermion loops, counter-clockwise diagrams should be included.

The CP violated htt coupling has been bounded as $|\tilde{\kappa}_t| < 0.01$ [56], which comes from the ACME experiment with the electron EDM limit $|d_e| < 8.7 \times 10^{-29} e \cdot \text{cm}$ [57]. Currently, the limit is improved to be $|d_e| < 1.1 \times 10^{-29} e \cdot \text{cm}$ [58]; then, we can rescale the limit of $\tilde{\kappa}_t$ as $|\tilde{\kappa}_t| < 1.26 \times 10^{-3}$. From a naive analog, the constraints on FCNY couplings are typically $1.26 \times 10^{-3}/\lambda^2 \sim \mathcal{O}(0.1)$. But this argument is not persuasive, because the two-loop results are unknown for these FCN coupling mediated diagrams. Therefore, we need to resort to other methods.

Secondly, the FCN couplings can be constrained from top quark EDM and CEDM. The top quark EDM is constrained to be $|d_t^{EDM}| < 5 \times 10^{-20} e \cdot \text{cm}$ at 90% CL [59–63] with the ACME results [57]. Similarly, we can rescale the limit of the top quark EDM to be $|d_t^{EDM}| < 6.3 \times 10^{-21} e \cdot \text{cm}$ or $|m_t d_t^{EDM}/e| < 5.5 \times 10^{-5}$ with the improved data [58]. The severe constraint on top quark CEDM is inferred from the neutron EDM with the magnitude of $|d_t^{CEDM}| < 2.1 \times 10^{-19} \text{cm}$ or $|m_t d_t^{CEDM}| < 1.9 \times 10^{-3}$ at 90% CL [61–66]. In the right diagram of Fig. 4, we show the Feynman diagram contributing to the top quark EDM. When the photon is replaced by a gluon, we can get the contribution to top CEDM. The interactions induced at one-loop have the following form:

$$\mathcal{L} \supset -\frac{i}{2} d_t^{EDM} \bar{t} \sigma^{\mu\nu} \gamma^5 t F_{\mu\nu} - \frac{i g_s}{2} d_t^{CEDM} \bar{t} \sigma^{\mu\nu} t^a \gamma^5 t G_{\mu\nu}^a. \quad (18)$$

The expressions of d_t^{EDM} and d_t^{CEDM} are computed as

$$d_t^{EDM} = \frac{e Q_T m_T [y_R^{tT} (y_L^{tT})^* - y_L^{tT} (y_R^{tT})^*]}{16\pi^2} C_1, \quad d_t^{CEDM} = \frac{m_T [y_R^{tT} (y_L^{tT})^* - y_L^{tT} (y_R^{tT})^*]}{16\pi^2} C_1, \quad (19)$$

where C_1 is defined as

$$C_1 = \frac{1}{4m_t^2} [B_0(m_t^2, m_T^2, m_h^2) - B_0(0, m_T^2, m_T^2) + (m_T^2 - m_t^2 - m_h^2) C_0(m_t^2, 0, m_t^2, m_h^2, m_T^2, m_T^2)].$$

$[y_R^{tT} (y_L^{tT})^* - y_L^{tT} (y_R^{tT})^*]$ can also be rewritten as $2i(\text{Re} y_L^{tT} \text{Im} y_R^{tT} - \text{Re} y_R^{tT} \text{Im} y_L^{tT})$; thus, d_t^{EDM} , d_t^{CEDM} will vanish if the imaginary parts of $y_{L,R}^{tT}$ are both turned off. If we take $m_T = 700$ GeV, top EDM and CEDM set the upper limits of $|y_R^{tT} (y_L^{tT})^* - y_L^{tT} (y_R^{tT})^*|$ to be 0.21 and 4.9, respectively. If we take $m_T = 400$ GeV, the corresponding upper limits of $|y_R^{tT} (y_L^{tT})^* - y_L^{tT} (y_R^{tT})^*|$ are 0.12 and 2.8, respectively. Thus, top quark EDM will give much stronger constraints than top CEDM.

IV. PARTIAL DECAY WIDTH FORMULA OF $h \rightarrow \gamma Z$

IV.1. SM result

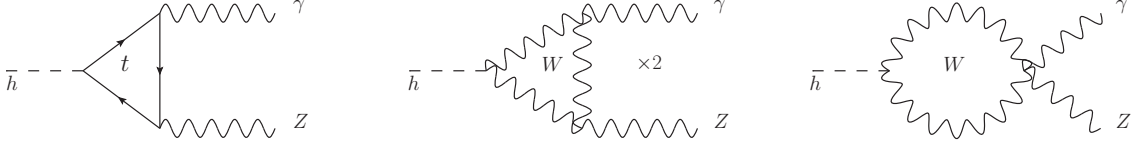


FIG. 5. Typical Feynman diagrams contributing to $h \rightarrow \gamma Z$ decay in the SM. For the fermion loops, counter-clockwise diagrams should be included.

There are contributions from top and W loops for the $h \rightarrow \gamma Z$ decay. In Fig. 5, we show the Feynman diagrams drawn by JaxoDraw [67]. The partial decay width in SM is computed as [68–72]

$$\Gamma^{SM}(h \rightarrow \gamma Z) = \frac{G_F \alpha^2 m_h^3}{64\sqrt{2}\pi^3} \left(1 - \frac{m_Z^2}{m_h^2}\right)^3 \left| \sum_f (2N_f^C Q_f) \frac{I_3^f - 2Q_f s_W^2}{s_W c_W} A_f(\tau_f, \lambda_f) + A_W(\tau_W, \lambda_W) \right|^2. \quad (20)$$

Here, τ_i and λ_i are defined as

$$\tau_f = \frac{4m_f^2}{m_h^2}, \tau_W = \frac{4m_W^2}{m_h^2}, \lambda_f = \frac{4m_f^2}{m_Z^2}, \lambda_W = \frac{4m_W^2}{m_Z^2}. \quad (21)$$

and the A_f, A_W are defined as

$$\begin{aligned} A_f(\tau_f, \lambda_f) &\equiv I_1(\tau_f, \lambda_f) - I_2(\tau_f, \lambda_f), \\ A_W(\tau_W, \lambda_W) &\equiv \frac{1}{t_W} \left\{ \left[\left(1 + \frac{2}{\tau_W}\right) t_W^2 - \left(5 + \frac{2}{\tau_W}\right) \right] I_1(\tau_W, \lambda_W) + 4(3 - t_W^2) I_2(\tau_W, \lambda_W) \right\}, \\ I_1(\tau, \lambda) &= \frac{\tau \lambda}{2(\tau - \lambda)} + \frac{\tau^2 \lambda^2}{2(\tau - \lambda)^2} [f(\tau) - f(\lambda)] + \frac{\tau^2 \lambda}{(\tau - \lambda)^2} [g(\tau) - g(\lambda)], \\ I_2(\tau, \lambda) &= -\frac{\tau \lambda}{2(\tau - \lambda)} [f(\tau) - f(\lambda)]. \end{aligned} \quad (22)$$

Here, $f(\tau)$ is given in App. B and $g(\tau)$ is defined as

$$g(\tau) \equiv \begin{cases} \sqrt{\tau - 1} \arcsin\left(\frac{1}{\sqrt{\tau}}\right), & \text{for } \tau \geq 1 \\ \frac{1}{2}\sqrt{1 - \tau} \left[\log \frac{1 + \sqrt{1 - \tau}}{1 - \sqrt{1 - \tau}} - i\pi \right], & \text{for } \tau < 1 \end{cases}. \quad (23)$$

The fermionic part is dominated by the top quark because of the largest Yukawa coupling. Numerically, we can get $(2N_t^C Q_t) \frac{I_3^t - 2Q_t s_W^2}{s_W c_W} A_f(\tau_t, \lambda_t) \sim -0.65$, $A_W(\tau_W, \lambda_W) \sim 12.03$, which means the gauge boson contributions are almost 18.5 times larger than the fermionic ones. It is obvious that the fermionic part and gauge boson part interfere destructively in the SM.

IV.2. New physics result

$h \rightarrow \gamma Z$ decay has already been considered in many models, for example, composite Higgs models [73, 74], minimal supersymmetric standard model (MSSM) [75, 76], next-to-MSSM (NMSSM) [76, 77], extended scalar sector models [14, 78, 79], and other new physics models [80]. In VLQ models, there are additional fermion contributions: pure new quark loops, loops with both SM and new quarks (see Fig. 6). The latter will be induced by the FCN interactions. Such off-diagonal contributions are always ignored in most studies [70, 73], because they are small compared to the diagonal terms. As a second thought, this channel can be sensitive to large non-diagonal couplings. Here, we do not enumerate models with more fermions, where the effects of non-diagonal couplings will be diluted or concealed. Besides, we only focus on the cases in which the scalar sector is extended with real gauge singlet scalars. In more complex scalar sector models, the charged Higgs contributions will also attenuate the flavour off-diagonal contributions.

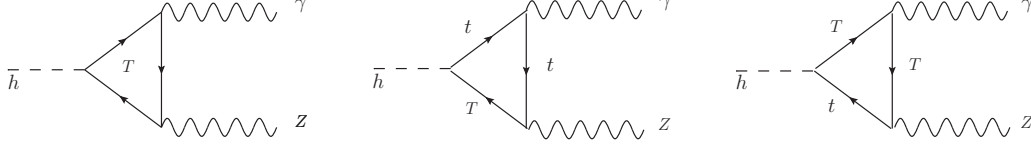


FIG. 6. Possible new fermion contributions to the $h \rightarrow \gamma Z$ decay. For the fermion loops, counter-clockwise diagrams should be included.

Now, let us consider the partial decay width of $h \rightarrow \gamma Z$ with the general interactions in Eq. (11). Due to $U_{EM}(1)$ gauge symmetry, the $h \rightarrow \gamma Z$ amplitude possesses the following tensor structure⁶:

$$i\mathcal{M} = i\epsilon_\mu(p_1)\epsilon_\nu(p_2)[(p_2^\mu p_1^\nu - p_1 \cdot p_2 g^{\mu\nu})\mathcal{A} + \epsilon^{\mu\nu p_1 p_2} B] \quad (\epsilon^{\mu\nu p_1 p_2} \equiv \epsilon^{\mu\nu\rho\sigma} p_{1,\rho} p_{2,\sigma}),$$

$$\mathcal{A} \equiv \frac{e^2}{8\pi^2 v}(\mathcal{A}_W + \mathcal{A}_t + \mathcal{A}_T + \mathcal{A}_{tT}), \quad \mathcal{B} \equiv \frac{e^2}{8\pi^2 v}\mathcal{B}_{tT}, \quad (24)$$

where $\mathcal{A}_W, \mathcal{A}_t, \mathcal{A}_T, \mathcal{A}_{tT}$ denote the contributions from W boson, top quark, T quark and $t - T$ mixed loops, respectively. Their expressions are given as

$$\mathcal{A}_W = A_W(\tau_W, \lambda_W),$$

$$\mathcal{A}_t = 2N_t^C Q_t (g_L^t + g_R^t) \kappa_t A_f(\tau_t, \lambda_t) = 2N_t^C Q_t \kappa_t \frac{\frac{1}{2}c_L^2 - \frac{4}{3}s_W^2}{s_W c_W} A_f(\tau_t, \lambda_t),$$

$$\mathcal{A}_T = -2N_T^C Q_T \frac{y_T v}{m_T} (g_L^T + g_R^T) A_f(\tau_T, \lambda_T) = -2N_T^C Q_T \frac{y_T v}{m_T} \frac{\frac{1}{2}s_L^2 - \frac{4}{3}s_W^2}{s_W c_W} A_f(\tau_T, \lambda_T),$$

⁶ During the calculations, we have used the FeynCalc to simplify the results [81, 82].

$$\begin{aligned}
\mathcal{A}_{tT} = & -4N_T^C Q_T g_L^{tT} \frac{v}{m_h^2 - m_Z^2} \{m_t \text{Re}(y_L^{tT}) [(\frac{m_h^2 - m_Z^2}{2} - m_t^2) C_0(0, m_Z^2, m_h^2, m_t^2, m_t^2, m_T^2) \\
& - m_T^2 C_0(0, m_Z^2, m_h^2, m_T^2, m_T^2, m_t^2) - m_Z^2 \frac{B_0(m_h^2, m_t^2, m_T^2) - B_0(m_Z^2, m_t^2, m_T^2)}{m_h^2 - m_Z^2} - 1] \\
& + m_T \text{Re}(y_R^{tT}) [(\frac{m_h^2 - m_Z^2}{2} - m_T^2) C_0(0, m_Z^2, m_h^2, m_T^2, m_T^2, m_t^2) \\
& - m_t^2 C_0(0, m_Z^2, m_h^2, m_t^2, m_t^2, m_T^2) - m_Z^2 \frac{B_0(m_h^2, m_t^2, m_T^2) - B_0(m_Z^2, m_t^2, m_T^2)}{m_h^2 - m_Z^2} - 1]\}. \quad (25)
\end{aligned}$$

Similarly, the expression of \mathcal{B}_{tT} is given as

$$\mathcal{B}_{tT} = -2N_T^C Q_T g_L^{tT} v [m_t \text{Im}(y_L^{tT}) C_0(0, m_Z^2, m_h^2, m_t^2, m_t^2, m_T^2) - m_T \text{Im}(y_R^{tT}) C_0(0, m_Z^2, m_h^2, m_T^2, m_T^2, m_t^2)]. \quad (26)$$

Taking the mass of t, T quarks to be infinity, $\mathcal{A}_t, \mathcal{A}_T$ can be expanded as

$$\begin{aligned}
\mathcal{A}_t & \approx -\frac{2}{3} N_t^C Q_t \kappa_t \frac{\frac{1}{2} c_L^2 - \frac{4}{3} s_W^2}{s_W c_W} [1 + \frac{7m_h^2 + 11m_Z^2}{120m_t^2} + \mathcal{O}(\frac{m_h^4, m_h^2 m_Z^2, m_Z^4}{m_t^4})], \\
\mathcal{A}_T & \approx -\frac{2}{3} N_T^C Q_T (-\frac{y_T v}{m_T}) \frac{\frac{1}{2} s_L^2 - \frac{4}{3} s_W^2}{s_W c_W} [1 + \frac{7m_h^2 + 11m_Z^2}{120m_T^2} + \mathcal{O}(\frac{m_h^4, m_h^2 m_Z^2, m_Z^4}{m_T^4})], \\
\mathcal{A}_t + \mathcal{A}_T & \approx -\frac{2N_T^C Q_T}{3s_W c_W} \left[\kappa_t (\frac{1}{2} c_L^2 - \frac{4}{3} s_W^2) (1 + \frac{7m_h^2 + 11m_Z^2}{120m_t^2}) + (-\frac{y_T v}{m_T}) (\frac{1}{2} s_L^2 - \frac{4}{3} s_W^2) (1 + \frac{7m_h^2 + 11m_Z^2}{120m_T^2}) \right]. \quad (27)
\end{aligned}$$

For the $\frac{1}{m_{t,T}^2}$ suppressed contributions, we can get $\frac{7m_h^2 + 11m_Z^2}{120m_t^2} \approx 5.5\%$, $\frac{7m_h^2 + 11m_Z^2}{120m_T^2} \lesssim 1\%$ if $m_T \gtrsim 400\text{GeV}$. The expansion of A_{tT} is a little bit complicated:

$$\begin{aligned}
\mathcal{A}_{tT} & \approx -4N_T^C Q_T g_L^{tT} \frac{v}{m_h^2 - m_Z^2} \{m_t \text{Re}(y_L^{tT}) [\frac{m_h^2 - m_Z^2}{m_T^2} \frac{(1 - r_{tT}^2)(3 - r_{tT}^2) + 2 \log r_{tT}^2}{4(1 - r_{tT}^2)^3} + \mathcal{O}(\frac{m_h^4, m_h^2 m_Z^2, m_Z^4}{m_t^4, m_t^2 m_T^2, m_T^4})] \\
& + m_T \text{Re}(y_R^{tT}) [\frac{m_h^2 - m_Z^2}{m_T^2} \frac{2r_{tT}^4 \log r_{tT}^2 - (1 - r_{tT}^2)(1 - 3r_{tT}^2)}{4(1 - r_{tT}^2)^3} + \mathcal{O}(\frac{m_h^4, m_h^2 m_Z^2, m_Z^4}{m_t^4, m_t^2 m_T^2, m_T^4})]\} \\
& \approx -N_T^C Q_T g_L^{tT} \frac{v}{m_T^2} [m_t \text{Re}(y_L^{tT}) (3 + 2 \log r_{tT}^2) - m_T \text{Re}(y_R^{tT})]. \quad (28)
\end{aligned}$$

Similarly, we can expand B_{tT} as

$$\begin{aligned}
\mathcal{B}_{tT} & \approx -2N_T^C Q_T g_L^{tT} \frac{v}{m_T^2} \{m_t \text{Im}(y_L^{tT}) [1 + \log r_{tT}^2 + \frac{m_h^2 + m_Z^2}{m_T^2} \frac{5 + 2(1 + 2r_{tT}^2) \log r_{tT}^2}{4}] \\
& + m_T \text{Im}(y_R^{tT}) [1 + r_{tT}^2 \log r_{tT}^2 + \frac{m_h^2 + m_Z^2}{m_T^2} \frac{1 + 4r_{tT}^2 \log r_{tT}^2}{4}]\}. \quad (29)
\end{aligned}$$

In Tab. III, we list the expressions of $A_t + A_T, A_{tT}, B_{tT}$ in three models, where we have neglected the $\frac{1}{m_{t,T}^2}$ suppressed terms but keep the $\log r_{tT}^2$ enhanced terms.

The partial decay width formula is computed as

$$\Gamma(h \rightarrow \gamma Z) = \frac{G_F \alpha^2 m_h^3}{64\sqrt{2}\pi^3} (1 - \frac{m_Z^2}{m_h^2})^3 [|A_t + A_T + A_{tT} + A_W(\tau_W, \lambda_W)|^2 + |\mathcal{B}_{tT}|^2]. \quad (30)$$

	$\bar{A}_t + \bar{A}_T$	\bar{A}_{tT}	\bar{B}_{tT}
SM	$1 - \frac{8}{3}s_W^2$	\times	\times
VLQT	$1 - \frac{8}{3}s_W^2 - 2s_L^2 c_L^2$	$\frac{3}{2}s_L^2 c_L^2 [1 - r_{tT}^2 (3 + 2 \log r_{tT}^2)]$	0
VLQT+S	$c_\theta (1 - \frac{8}{3}s_W^2 - 2s_L^2 c_L^2) + \frac{v \text{Re}(y_T^S)}{m_T} \frac{s_\theta c_R}{c_L} (\frac{8}{3}s_W^2 - 2s_L^2 c_L^2)$	$\frac{3}{2}s_L c_L [s_L c_L c_\theta (1 - r_{tT}^2 (3 + 2 \log r_{tT}^2)) + \frac{v \text{Re}(y_T^S)}{m_T} s_\theta (s_L c_R - r_{tT} (3 + 2 \log r_{tT}^2) s_{RCL})]$	$-\frac{3v}{m_T} s_L^2 c_L c_R s_\theta \text{Im}(y_T^S)$

TABLE III. The expressions of $\bar{A}_t + \bar{A}_T, \bar{A}_{tT}, \bar{B}_{tT}$ in the SM, VLQT, and VLQT+S. Here, we extract the common factor $-\frac{N_T^C Q_T}{3s_W c_W}$ for convenience, that is, redefinition of $A(B)$ with $-\frac{N_T^C Q_T}{3s_W c_W} \bar{A}(\bar{B})$. We take $\bar{A}_T = 0$ naively in SM because of the absence of a T quark.

IV.3. Comments from the viewpoint of low energy theorem

As a matter of fact, we can also understand some behaviors of the $h \rightarrow \gamma Z$ amplitude resorting to the low energy theorem [83, 84]. Just as the calculation of $h \rightarrow \gamma\gamma$ amplitude from photon self-energy contribution [85, 86], we may get the $h \rightarrow \gamma Z$ amplitude through $\gamma - Z$ mixed self-energy contribution [87]. But what confuses us is that there seems no off-diagonal fermion contributions to the $\gamma - Z$ two-point function because photon can only couple to the same flavour particle. The reason is that off-diagonal couplings are proportional to the mixing angle, which is suppressed by the heavy fermion mass. Thus, off-diagonal contributions to the $h \rightarrow \gamma Z$ amplitude vanish in the limit of $p_h \rightarrow 0$, consistent with the corollary of low energy theorem. In other words, this channel will give looser constraints on off-diagonal couplings once one flavour of the loop particles becomes heavier.

V. NUMERICAL RESULTS AND CONSTRAINT PROSPECTS

Just similar to the VLQT model, we take $\kappa_t = c_L^2, y_T = -\frac{m_T}{v} s_L^2$ for simplicity, but let $\text{Re}(y_L^{tT}), \text{Re}(y_R^{tT}), \text{Im}(y_L^{tT}), \text{Im}(y_R^{tT})$ be free. Then, we can choose several benchmark scenarios and estimate the constraints on the magnitude and sign of the FCNY couplings.

Since the branching ratio of $h \rightarrow \gamma Z$ is about 1.5×10^{-3} , the modification of $h\gamma Z$ partial decay width will cause negligible effects on the Higgs total width. At the high luminosity LHC (HL-LHC), $h\gamma Z$ coupling can be measured accurately [88, 89]. The expected 1σ uncertainty of $Br(h \rightarrow \gamma Z)$ is 19.1% [88], which gives the following constraint:

$$|\Gamma(h \rightarrow \gamma Z)/\Gamma^{SM}(h \rightarrow \gamma Z) - 1| \leq 19.1\%. \quad (31)$$

It means $||A|^2 + |B|^2|/|A^{SM}|^2 - 1| \leq 19.1\%$. From now on, we will choose $m_T = 400$ GeV and $s_L = 0.2$. As mentioned above, there are four interesting parameters: $\text{Re}(y_L^{tT}), \text{Re}(y_R^{tT}), \text{Im}(y_L^{tT}), \text{Im}(y_R^{tT})$. In the following, we will plot the reached two-dimensional parameter space by setting two of them to be zeros or imposing two conditions.

In Fig. 7, we plot the parameter space regions allowed by perturbative unitarity in Eq. (13) and the expected constraints at HL-LHC in Eq. (31) in different scenarios. The reach regions are shown in blue at 1σ CL, and the 2σ bounds in $h \rightarrow \gamma Z$ decay are weaker than the unitarity constraints. When evaluating the scalar loop functions, LoopTools is employed [90]. In the first plot, we can find that $h \rightarrow \gamma Z$ decay gives a little stronger constraints than perturbative unitarity in the first and third quadrants in the case of vanishing imaginary parts of y_L^{tT}, y_R^{tT} . In the presence of imaginary

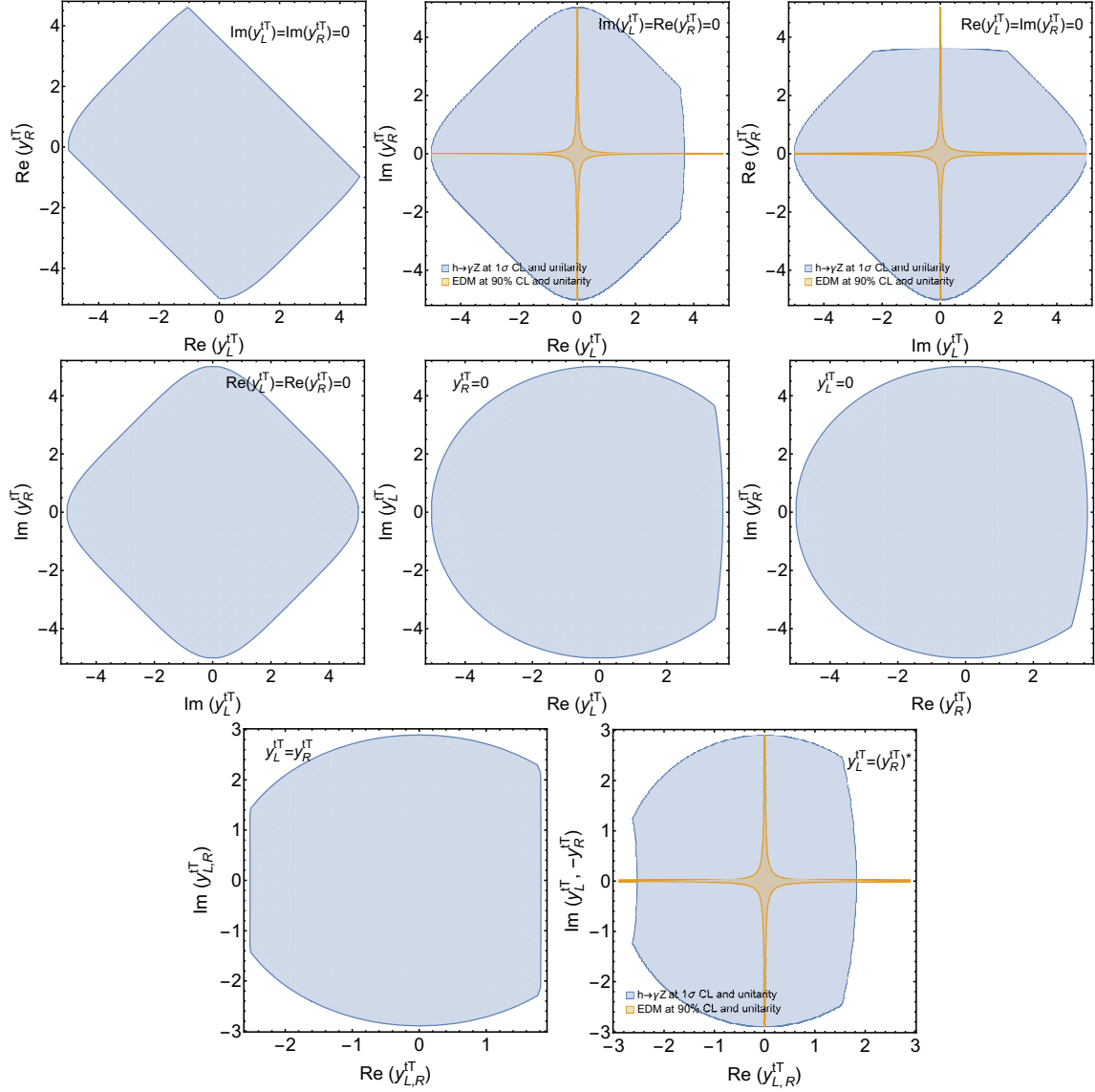


FIG. 7. The reach regions of y_L^{tT} , y_R^{tT} in several scenarios. In the above plots, we take $\text{Im}(y_L^{tT}) = \text{Im}(y_R^{tT}) = 0$ (upper left), $\text{Im}(y_L^{tT}) = \text{Re}(y_R^{tT}) = 0$ (upper central), $\text{Re}(y_L^{tT}) = \text{Im}(y_R^{tT}) = 0$ (upper right), $\text{Re}(y_L^{tT}) = \text{Re}(y_R^{tT}) = 0$ (middle left), $y_R^{tT} = 0$ (middle central), $y_L^{tT} = 0$ (middle right), $y_L^{tT} = y_R^{tT}$ (lower left) and $y_L^{tT} = (y_R^{tT})^*$ (lower right), respectively. Here only the three scenarios $\text{Im}(y_L^{tT}) = \text{Re}(y_R^{tT}) = 0$, $\text{Re}(y_L^{tT}) = \text{Im}(y_R^{tT}) = 0$, and $y_L^{tT} = (y_R^{tT})^*$ can be constrained by the top quark EDM constraints. The blue region means that it can be reached by the $h \rightarrow \gamma Z$ decay at 1σ CL and allowed by the unitarity bounds, and the yellow region means that it is allowed by the EDM at 90% CL and unitarity bounds.

part, the real part can be constrained to be less than 3 roughly in the positive direction, while

it will give a looser bound than the unitary constraints in the negative direction. In the case of vanishing real parts of y_L^{tT}, y_R^{tT} , the imaginary parts can only be constrained by unitarity. When the couplings are pure left or pure right, the real parts are also constrained to be less than 3 roughly in the positive direction. For the cases of equal or conjugate y_L^{tT}, y_R^{tT} , the real parts can be bounded to be less than 1.5 in the positive direction and greater than -3 in the negative direction.

As a matter of fact, the behaviours in Fig. 7 can be explained by the results in Sec. IV.2 qualitatively. In $|A_t + A_T + A_{tT} + A_W(\tau_W, \lambda_W)|^2$, A_{tT} can interfere constructively or destructively with $A_W(\tau_W, \lambda_W)$, while $|\mathcal{B}_{tT}|^2$ always enhances the partial width. It will give strong constraints for the constructive case because of double enhancement from A_{tT}, B_{tT} . A_{tT} is proportional to real parts of $y_{L,R}^{tT}$, while B_{tT} receives the contribution from the imaginary parts of $y_{L,R}^{tT}$. Thus, real parts of $y_{L,R}^{tT}$ are more tightly constrained than the imaginary parts because of the interference with the large $A_W(\tau_W, \lambda_W)$ term. If $A_{tT} > 0$ (or $[m_T \text{Re}(y_R^{tT}) - (3 + 2 \log r_{tT}^2) m_t \text{Re}(y_L^{tT})] > 0$), it will interfere constructively with $A_W(\tau_W, \lambda_W)$. The appearance of B_{tT} will enhance the partial width further; thus, this case is more strongly bounded. If $A_{tT} < 0$, there will be some cancellation between the destructive interference with $A_W(\tau_W, \lambda_W)$ and the enhancement from B_{tT} . Thus, this case is more loosely bounded.

Although the $m_t y_L^{tT}$ term is suppressed by the factor $\frac{m_t}{m_T}$ compared to the $m_T y_R^{tT}$ term, it is $\log r_{tT}^2$ enhanced. Thus, we should take both of them into account. Because of $A_{tT} \sim [m_T \text{Re}(y_R^{tT}) - (3 + 2 \log r_{tT}^2) m_t \text{Re}(y_L^{tT})]$, the regions of $\text{Re}(y_L^{tT}), \text{Re}(y_R^{tT})$ with same sign are more strongly bounded than those with opposite sign. Because of $\mathcal{B}_{tT} \sim [m_t(1 + \log r_{tT}^2) \text{Im}(y_L^{tT}) + m_T \text{Im}(y_R^{tT})]$, the regions of $\text{Im}(y_L^{tT}), \text{Im}(y_R^{tT})$ with opposite sign are more strongly bounded than those with same sign (compare $y_L^{tT} = y_R^{tT}$ case with the $y_L^{tT} = (y_R^{tT})^*$ case in Fig. 7).

Although the attempts show that the constraints are quite loose, it is still worth investigating the FCNY couplings through the $h \rightarrow \gamma Z$ decay mode. The contributions of FCN couplings are suppressed by both s_L and $\frac{v}{m_T}$. If s_L is not very small, it can give considerable constraints on the FCNY couplings. When s_L becomes very small (say $s_L = 0.1$), $h \rightarrow \gamma Z$ decay will lose the power to constrain FCNY couplings (looser than the perturbative unitarity bound). When m_T becomes very heavy (say TeV), it will also lose the power to constrain FCNY couplings.

In Sec. III.6, we have illustrated that the top quark EDM may give some bounds on the FCNY couplings. Because we have the identity $y_R^{tT}(y_L^{tT})^* - y_L^{tT}(y_R^{tT})^* = 2i(\text{Re} y_L^{tT} \text{Im} y_R^{tT} - \text{Re} y_R^{tT} \text{Im} y_L^{tT})$, the blind directions from top EDM are $y_L^{tT} = 0, y_R^{tT} = 0, y_L^{tT} = y_R^{tT}, \text{Im} y_L^{tT} = \text{Im} y_R^{tT} = 0, \text{Re} y_L^{tT} = \text{Re} y_R^{tT} = 0$. For the three cases $\text{Im}(y_L^{tT}) = \text{Re}(y_R^{tT}) = 0, \text{Re}(y_L^{tT}) = \text{Im}(y_R^{tT}) = 0, y_L^{tT} = (y_R^{tT})^*$, the top quark EDM can give strong constraints. In Fig. 7, we also show the allowed regions from top quark EDM at 90% CL and perturbative unitarity (yellow) for these three scenarios. From these plots, we can find that the off-axis regions are strongly bounded by top EDM, while it loses the constraining power in the near axis regions.

By the way, $h \rightarrow \gamma\gamma$ depends only on the same flavour Yukawa couplings, while $h \rightarrow \gamma Z$ decay is also controlled by the FCN couplings. By combining $h \rightarrow \gamma\gamma, \gamma Z$ together, it is possible to disentangle the FCNY couplings from the same flavour Yukawa couplings. For the doublet and triplets VLQ cases, there are extra heavy quarks besides the $T_{L,R}$. The new heavy quarks can contribute to the $h \rightarrow \gamma Z$ decay; thus, the FCNY coupling constraints will be quite loose. Certainly, the FCN couplings can show up in other processes, too. For example, we can search for new physics through the di-Higgs production [91–93], while the $gg \rightarrow hh$ process suffers from the anomalous hhh coupling. The $e^+e^- \rightarrow h\gamma$ production at electron-positron colliders is also an interesting process and it has drawn much attention of the community. It can also be a probe of the anomalous $h\gamma Z$ and $h\gamma\gamma$ couplings. The SM analysis for this process is given in Refs. [94–96]. There are also some works on this process in many new physics models, for example, the MSSM [96–99], extended scalar sector

models [100, 101], VLQ models [102], effective field theory framework [103–106], and simplified scenarios [107]. Besides, we can also probe the FCNY couplings through direct production processes $pp \rightarrow Tth, Tt, ThW, Thj$. But they suffer from a low event rate. Although the FCNY couplings may also be constrained from other processes, the detailed analyses in these channels are beyond the scope of this work.

VI. SUMMARY AND CONCLUSIONS

There can exist FCN interactions between the top quark and new heavy quark. To unravel the nature of flavour structure and EWSB, it is of great importance to probe such couplings. Unfortunately, it is difficult to constrain the FCN couplings at both current and future experiments. Here, we show how to bound the FCNY couplings in simplified singlet T_L, T_R extended models generally.

In this paper, we have summarized the main constraints from theoretical and experimental viewpoints. By turning off other couplings naively, we get the perturbative unitarity bounds on $|y_{L,R}^{tT}|$. After considering the constraints from direct search, S, T parameters, top physics, and Higgs signal strength, we take $m_T = 400$ GeV and $s_L = 0.2$ as the benchmark point to get the optimal situation. Under this benchmark point, we consider the future bounds from $h \rightarrow \gamma Z$ decay at HL-LHC numerically. The real parts of $y_{L,R}^{tT}$ in the positive direction can be limited to be less than $1.5 \sim 3$ because of the double enhancement. For the real parts of $y_{L,R}^{tT}$ in the negative direction, they are mainly bounded by the perturbative unitarity. Finally, we find that top quark EDM can give stronger bounds (especially the imaginary parts of $y_{L,R}^{tT}$) than the perturbative unitarity and $h \rightarrow \gamma Z$ decay in the off-axis regions for some scenarios.

ACKNOWLEDGMENTS

We would like to thank Gang Li, Zhao Li, Ying-nan Mao, Cen Zhang, and Hao Zhang for helpful discussions. We also thank Jordy de Vries for directing our attention to the latest constraints on top quark EDM.

-
- [1] S. L. Glashow. Partial Symmetries of Weak Interactions. *Nucl. Phys.*, 22:579–588, 1961.
Steven Weinberg. A Model of Leptons. *Phys. Rev. Lett.*, 19:1264–1266, 1967.
Abdus Salam. Weak and Electromagnetic Interactions. *Conf. Proc.*, C680519:367–377, 1968.
 - [2] Kaustubh Agashe, Roberto Contino, and Alex Pomarol. The Minimal composite Higgs model. *Nucl. Phys.*, B719:165–187, 2005.
 - [3] Giuliano Panico and Andrea Wulzer. The Composite Nambu-Goldstone Higgs. *Lect. Notes Phys.*, 913:pp.1–316, 2016.
 - [4] N. Arkani-Hamed, A. G. Cohen, E. Katz, and A. E. Nelson. The Littlest Higgs. *JHEP*, 07:034, 2002.
 - [5] Martin Schmaltz and David Tucker-Smith. Little Higgs review. *Ann. Rev. Nucl. Part. Sci.*, 55:229–270, 2005.
 - [6] JoAnne L. Hewett and Thomas G. Rizzo. Low-Energy Phenomenology of Superstring Inspired E(6) Models. *Phys. Rept.*, 183:193, 1989.
 - [7] Roberto Contino, Thomas Kramer, Minho Son, and Raman Sundrum. Warped/composite phenomenology simplified. *JHEP*, 05:074, 2007.

- [8] Georges Aad et al. Observation of a new particle in the search for the Standard Model Higgs boson with the ATLAS detector at the LHC. *Phys. Lett.*, B716:1–29, 2012.
Serguei Chatrchyan et al. Observation of a new boson at a mass of 125 GeV with the CMS experiment at the LHC. *Phys. Lett.*, B716:30–61, 2012.
- [9] F. Englert and R. Brout. Broken Symmetry and the Mass of Gauge Vector Mesons. *Phys. Rev. Lett.*, 13:321–323, 1964.
Peter W. Higgs. Broken symmetries, massless particles and gauge fields. *Phys. Lett.*, 12:132–133, 1964.
G. S. Guralnik, C. R. Hagen, and T. W. B. Kibble. Global Conservation Laws and Massless Particles. *Phys. Rev. Lett.*, 13:585–587, 1964.
T. W. B. Kibble. Symmetry breaking in nonAbelian gauge theories. *Phys. Rev.*, 155:1554–1561, 1967.
- [10] S. Dittmaier et al. Handbook of LHC Higgs Cross Sections: 1. Inclusive Observables. 2011.
S. Dittmaier et al. Handbook of LHC Higgs Cross Sections: 2. Differential Distributions. 2012.
J R Andersen et al. Handbook of LHC Higgs Cross Sections: 3. Higgs Properties. 2013.
D. de Florian et al. Handbook of LHC Higgs Cross Sections: 4. Deciphering the Nature of the Higgs Sector. 2016.
- [11] Yi Chen, Adam Falkowski, Ian Low, and Roberto Vega-Morales. New Observables for CP Violation in Higgs Decays. *Phys. Rev.*, D90(11):113006, 2014.
- [12] Marco Farina, Yuval Grossman, and Dean J. Robinson. Probing CP violation in $h \rightarrow Z\gamma$ with background interference. *Phys. Rev.*, D92(7):073007, 2015.
- [13] Xuan Chen, Gang Li, and Xia Wan. Probe CP violation in $H \rightarrow \gamma Z$ through forward-backward asymmetry. *Phys. Rev.*, D96(5):055023, 2017.
- [14] Chian-Shu Chen, Chao-Qiang Geng, Da Huang, and Lu-Hsing Tsai. New Scalar Contributions to $h \rightarrow Z\gamma$. *Phys. Rev.*, D87:075019, 2013.
- [15] Jose Miguel No and Michael Spannowsky. A Boost to $h \rightarrow Z\gamma$: from LHC to Future e^+e^- Colliders. *Phys. Rev.*, D95(7):075027, 2017.
- [16] Sally Dawson and Pier Paolo Giardino. Higgs decays to ZZ and $Z\gamma$ in the standard model effective field theory: An NLO analysis. *Phys. Rev.*, D97(9):093003, 2018.
- [17] F. del Aguila, M. Perez-Victoria, and Jose Santiago. Effective description of quark mixing. *Phys. Lett.*, B492:98–106, 2000.
- [18] F. del Aguila, M. Perez-Victoria, and Jose Santiago. Observable contributions of new exotic quarks to quark mixing. *JHEP*, 09:011, 2000.
- [19] J. A. Aguilar-Saavedra. Effects of mixing with quark singlets. *Phys. Rev.*, D67:035003, 2003. [Erratum: *Phys. Rev.* D69,099901(2004)].
- [20] J. A. Aguilar-Saavedra. Identifying top partners at LHC. *JHEP*, 11:030, 2009.
- [21] J. A. Aguilar-Saavedra, R. Benbrik, S. Heinemeyer, and M. Pérez-Victoria. Handbook of vectorlike quarks: Mixing and single production. *Phys. Rev.*, D88(9):094010, 2013.
- [22] Hong-Jian He and Zhong-Zhi Xianyu. Extending Higgs Inflation with TeV Scale New Physics. *JCAP*, 10:019, 2014.
- [23] Matthew J. Dolan, J. L. Hewett, M. Krämer, and T. G. Rizzo. Simplified Models for Higgs Physics: Singlet Scalar and Vector-like Quark Phenomenology. *JHEP*, 07:039, 2016.
- [24] Jeong Han Kim and Ian M. Lewis. Loop Induced Single Top Partner Production and Decay at the LHC. *JHEP*, 05:095, 2018.
- [25] J. A. Aguilar-Saavedra, D. E. López-Fogliani, and C. Muñoz. Novel signatures for vector-like quarks. *JHEP*, 06:095, 2017.
- [26] Margarete Muhlleitner, Marco O. P. Sampaio, Rui Santos, and Jonas Wittbrodt. The N2HDM under Theoretical and Experimental Scrutiny. *JHEP*, 03:094, 2017.
- [27] Kingman Cheung, Shi-Ping He, Ying-nan Mao, Po-Yan Tseng, and Chen Zhang. Phenomenology of a little Higgs pseudoaxion. *Phys. Rev.*, D98(7):075023, 2018.
- [28] Giacomo Cacciapaglia, Thomas Flacke, Myeonghun Park, and Mengchao Zhang. Exotic decays of top partners: mind the search gap. *Phys. Lett. B*, 798:135015, 2019.
- [29] S. Dawson and E. Furlan. A Higgs Conundrum with Vector Fermions. *Phys. Rev.*, D86:015021, 2012.
- [30] Andrea De Simone, Oleksii Matsedonskyi, Riccardo Rattazzi, and Andrea Wulzer. A First Top Partner

- Hunter's Guide. *JHEP*, 04:004, 2013.
- [31] Ming-Lei Xiao and Jiang-Hao Yu. Stabilizing electroweak vacuum in a vectorlike fermion model. *Phys. Rev.*, D90(1):014007, 2014. [Addendum: *Phys. Rev.* D90,no.1,019901(2014)].
 - [32] Vernon Barger, Paul Langacker, Mathew McCaskey, Michael J. Ramsey-Musolf, and Gabe Shaughnessy. LHC Phenomenology of an Extended Standard Model with a Real Scalar Singlet. *Phys. Rev.*, D77:035005, 2008.
 - [33] Chien-Yi Chen, S. Dawson, and I. M. Lewis. Exploring resonant di-Higgs boson production in the Higgs singlet model. *Phys. Rev.*, D91(3):035015, 2015.
 - [34] Shinya Kanemura, Mariko Kikuchi, and Kei Yagyu. Radiative corrections to the Higgs boson couplings in the model with an additional real singlet scalar field. *Nucl. Phys.*, B907:286–322, 2016.
 - [35] Shi-Ping He and Shou-hua Zhu. One-Loop Radiative Correction to the Triple Higgs Coupling in the Higgs Singlet Model. *Phys. Lett.*, B764:31–37, 2017.
 - [36] Shinya Kanemura, Mariko Kikuchi, and Kei Yagyu. One-loop corrections to the Higgs self-couplings in the singlet extension. *Nucl. Phys.*, B917:154–177, 2017.
 - [37] Ian M. Lewis and Matthew Sullivan. Benchmarks for Double Higgs Production in the Singlet Extended Standard Model at the LHC. *Phys. Rev. D*, 96(3):035037, 2017.
 - [38] Mathieu Buchkremer, Giacomo Cacciapaglia, Aldo Deandrea, and Luca Panizzi. Model Independent Framework for Searches of Top Partners. *Nucl. Phys.*, B876:376–417, 2013.
 - [39] Benjamin W. Lee, C. Quigg, and H. B. Thacker. Weak Interactions at Very High-Energies: The Role of the Higgs Boson Mass. *Phys. Rev.*, D16:1519, 1977.
 - [40] Michael S. Chanowitz, M. A. Furman, and I. Hinchliffe. Weak Interactions of Ultraheavy Fermions. 2. *Nucl. Phys.*, B153:402–430, 1979.
 - [41] F. Maltoni, J. M. Niczyporuk, and S. Willenbrock. The Scale of fermion mass generation. *Phys. Rev.*, D65:033004, 2002.
 - [42] Duane A. Dicus and Hong-Jian He. Scales of fermion mass generation and electroweak symmetry breaking. *Phys. Rev. D*, 71:093009, 2005.
 - [43] Duane A. Dicus and Hong-Jian He. Scales of mass generation for quarks, leptons and majorana neutrinos. *Phys. Rev. Lett.*, 94:221802, 2005.
 - [44] Morad Aaboud et al. Combination of the searches for pair-produced vector-like partners of the third-generation quarks at $\sqrt{s} = 13$ TeV with the ATLAS detector. *Phys. Rev. Lett.*, 121(21):211801, 2018.
 - [45] Albert M Sirunyan et al. Search for pair production of vectorlike quarks in the fully hadronic final state. *Phys. Rev.*, D100(7):072001, 2019.
 - [46] Morad Aaboud et al. Search for single production of vector-like quarks decaying into Wb in pp collisions at $\sqrt{s} = 13$ TeV with the ATLAS detector. *JHEP*, 05:164, 2019.
 - [47] Michael E. Peskin and Tatsu Takeuchi. A New constraint on a strongly interacting Higgs sector. *Phys. Rev. Lett.*, 65:964–967, 1990.
 - [48] Michael E. Peskin and Tatsu Takeuchi. Estimation of oblique electroweak corrections. *Phys. Rev.*, D46:381–409, 1992.
 - [49] L. Lavoura and Joao P. Silva. The Oblique corrections from vector - like singlet and doublet quarks. *Phys. Rev.*, D47:2046–2057, 1993.
 - [50] Chien-Yi Chen, S. Dawson, and Elisabetta Furlan. Vectorlike fermions and Higgs effective field theory revisited. *Phys. Rev.*, D96(1):015006, 2017.
 - [51] M. Tanabashi et al. Review of Particle Physics. *Phys. Rev.*, D98(3):030001, 2018.
 - [52] Qing-Hong Cao, Bin Yan, Jiang-Hao Yu, and Chen Zhang. A General Analysis of Wtb anomalous Couplings. *Chin. Phys. C*, 41(6):063101, 2017.
 - [53] Vardan Khachatryan et al. Measurement of the t-channel single-top-quark production cross section and of the $|V_{tb}|$ CKM matrix element in pp collisions at $\sqrt{s} = 8$ TeV. *JHEP*, 06:090, 2014.
 - [54] Albert M Sirunyan et al. Combined measurements of Higgs boson couplings in proton–proton collisions at $\sqrt{s} = 13$ TeV. *Eur. Phys. J.*, C79(5):421, 2019.
- Georges Aad et al. Combined measurements of Higgs boson production and decay using up to 80 fb^{-1} of proton-proton collision data at $\sqrt{s} = 13$ TeV collected with the ATLAS experiment. *Phys. Rev. D*, 101(1):012002, 2020.

- [55] Stephen M. Barr and A. Zee. Electric Dipole Moment of the Electron and of the Neutron. *Phys. Rev. Lett.*, 65:21–24, 1990. [Erratum: *Phys. Rev. Lett.* 65, 2920(1990)].
- [56] Joachim Brod, Ulrich Haisch, and Jure Zupan. Constraints on CP-violating Higgs couplings to the third generation. *JHEP*, 11:180, 2013.
- [57] Jacob Baron et al. Order of Magnitude Smaller Limit on the Electric Dipole Moment of the Electron. *Science*, 343:269–272, 2014.
- [58] V. Andreev et al. Improved limit on the electric dipole moment of the electron. *Nature*, 562(7727):355–360, 2018.
- [59] Joanne L. Hewett and Thomas G. Rizzo. Using $b \rightarrow s \gamma$ to probe top quark couplings. *Phys. Rev.*, D49:319–322, 1994.
- [60] A. Cordero-Cid, J. M. Hernandez, G. Tavares-Velasco, and J. J. Toscano. Bounding the top and bottom electric dipole moments from neutron experimental data. *J. Phys.*, G35:025004, 2008.
- [61] Jernej F. Kamenik, Michele Papucci, and Andreas Weiler. Constraining the dipole moments of the top quark. *Phys. Rev.*, D85:071501, 2012. [Erratum: *Phys. Rev.* D88, no. 3, 039903(2013)].
- [62] V. Cirigliano, W. Dekens, J. de Vries, and E. Mereghetti. Is there room for CP violation in the top-Higgs sector? *Phys. Rev. D*, 94(1):016002, 2016.
- [63] V. Cirigliano, W. Dekens, J. de Vries, and E. Mereghetti. Constraining the top-Higgs sector of the Standard Model Effective Field Theory. *Phys. Rev. D*, 94(3):034031, 2016.
- [64] C.A. Baker et al. An Improved experimental limit on the electric dipole moment of the neutron. *Phys. Rev. Lett.*, 97:131801, 2006.
- [65] J. M. Pendlebury et al. Revised experimental upper limit on the electric dipole moment of the neutron. *Phys. Rev. D*, 92(9):092003, 2015.
- [66] Y.T. Chien, V. Cirigliano, W. Dekens, J. de Vries, and E. Mereghetti. Direct and indirect constraints on CP-violating Higgs-quark and Higgs-gluon interactions. *JHEP*, 02:011, 2016.
- [67] D. Binosi, J. Collins, C. Kaufhold, and L. Theussl. JaxoDraw: A Graphical user interface for drawing Feynman diagrams. Version 2.0 release notes. *Comput. Phys. Commun.*, 180:1709–1715, 2009.
- [68] L. Bergstrom and G. Hulth. Induced Higgs Couplings to Neutral Bosons in e^+e^- Collisions. *Nucl. Phys.*, B259:137–155, 1985. [Erratum: *Nucl. Phys.* B276, 744(1986)].
- [69] John F. Gunion, Howard E. Haber, Gordon L. Kane, and Sally Dawson. The Higgs Hunter’s Guide. *Front. Phys.*, 80:1–404, 2000.
- [70] A. Djouadi, V. Driesen, W. Hollik, and A. Kraft. The Higgs photon - Z boson coupling revisited. *Eur. Phys. J.*, C1:163–175, 1998.
- [71] Abdelhak Djouadi. The Anatomy of electro-weak symmetry breaking. I: The Higgs boson in the standard model. *Phys. Rept.*, 457:1–216, 2008.
- [72] I. Boradjiev, E. Christova, and H. Eberl. Dispersion theoretic calculation of the $H \rightarrow Z + \gamma$ amplitude. *Phys. Rev.*, D97(7):073008, 2018.
- [73] Aleksandr Azatov, Roberto Contino, Andrea Di Iura, and Jamison Galloway. New Prospects for Higgs Compositeness in $h \rightarrow Z\gamma$. *Phys. Rev.*, D88(7):075019, 2013.
- [74] Qing-Hong Cao, Ling-Xiao Xu, Bin Yan, and Shou-Hua Zhu. Signature of pseudo Nambu–Goldstone Higgs boson in its decay. *Phys. Lett.*, B789:233–237, 2019.
- [75] Abdelhak Djouadi. The Anatomy of electro-weak symmetry breaking. II. The Higgs bosons in the minimal supersymmetric model. *Phys. Rept.*, 459:1–241, 2008.
- [76] Junjie Cao, Lei Wu, Peiwen Wu, and Jin Min Yang. The Z+photon and diphoton decays of the Higgs boson as a joint probe of low energy SUSY models. *JHEP*, 09:043, 2013.
- [77] Genevieve Belanger, Vincent Bizouard, and Guillaume Chalons. Boosting Higgs boson decays into gamma and a Z in the NMSSM. *Phys. Rev.*, D89(9):095023, 2014.
- [78] Cheng-Wei Chiang and Kei Yagyu. Higgs boson decays to $\gamma\gamma$ and $Z\gamma$ in models with Higgs extensions. *Phys. Rev.*, D87(3):033003, 2013.
- [79] Bogumila Swiezewska and Maria Krawczyk. Diphoton rate in the inert doublet model with a 125 GeV Higgs boson. *Phys. Rev.*, D88(3):035019, 2013.
- [80] Chian-Shu Chen, Chao-Qiang Geng, Da Huang, and Lu-Hsing Tsai. $h \rightarrow Z\gamma$ in Type-II seesaw neutrino model. *Phys. Lett.*, B723:156–160, 2013.
- [81] R. Mertig, M. Bohm, and Ansgar Denner. FEYN CALC: Computer algebraic calculation of Feynman

- amplitudes. *Comput. Phys. Commun.*, 64:345–359, 1991.
- [82] Vladyslav Shtabovenko, Rolf Mertig, and Frederik Orellana. New Developments in FeynCalc 9.0. *Comput. Phys. Commun.*, 207:432–444, 2016.
 - [83] John R. Ellis, Mary K. Gaillard, and Dimitri V. Nanopoulos. A Phenomenological Profile of the Higgs Boson. *Nucl. Phys.*, B106:292, 1976.
 - [84] Mikhail A. Shifman, A. I. Vainshtein, M. B. Voloshin, and Valentin I. Zakharov. Low-Energy Theorems for Higgs Boson Couplings to Photons. *Sov. J. Nucl. Phys.*, 30:711–716, 1979. [*Yad. Fiz.*30,1368(1979)].
 - [85] Marcela Carena, Ian Low, and Carlos E. M. Wagner. Implications of a Modified Higgs to Diphoton Decay Width. *JHEP*, 08:060, 2012.
 - [86] Qing-Hong Cao, Yandong Liu, Ke-Pan Xie, Bin Yan, and Dong-Ming Zhang. Diphoton excess, low energy theorem, and the 331 model. *Phys. Rev. D*, 93(7):075030, 2016.
 - [87] Bernd A. Kniehl and Michael Spira. Low-energy theorems in Higgs physics. *Z. Phys.*, C69:77–88, 1995.
 - [88] M. Cepeda et al. *Report from Working Group 2: Higgs Physics at the HL-LHC and HE-LHC*, volume 7, pages 221–584. 12 2019.
 - [89] Florian Goertz, Eric Madge, Pedro Schwaller, and Valentin Titus Tenorth. Discovering the $h \rightarrow Z\gamma$ decay in $t\bar{t}$ associated production. *Phys. Rev. D*, 102(5):053004, 2020.
 - [90] T. Hahn and M. Perez-Victoria. Automatized one loop calculations in four-dimensions and D-dimensions. *Comput. Phys. Commun.*, 118:153–165, 1999.
 - [91] T. Plehn, M. Spira, and P. M. Zerwas. Pair production of neutral Higgs particles in gluon-gluon collisions. *Nucl. Phys.*, B479:46–64, 1996. [Erratum: *Nucl. Phys.*B531,655(1998)].
 - [92] Chih-Ting Lu, Jung Chang, Kingman Cheung, and Jae Sik Lee. An exploratory study of Higgs-boson pair production. *JHEP*, 08:133, 2015.
 - [93] Qing-Hong Cao, Gang Li, Bin Yan, Dong-Ming Zhang, and Hao Zhang. Double Higgs production at the 14 TeV LHC and a 100 TeV pp collider. *Phys. Rev.*, D96(9):095031, 2017.
 - [94] A. Barroso, J. Pulido, and J. C. Romao. HIGGS PRODUCTION AT $e^+ e^-$ COLLIDERS. *Nucl. Phys.*, B267:509–530, 1986.
 - [95] Ali Abbasabadi, David Bowser-Chao, Duane A. Dicus, and Wayne W. Repko. Higgs photon associated production at $e\bar{e}$ colliders. *Phys. Rev.*, D52:3919–3928, 1995.
 - [96] A. Djouadi, V. Driesen, W. Hollik, and J. Rosiek. Associated production of Higgs bosons and a photon in high-energy $e^+ e^-$ collisions. *Nucl. Phys.*, B491:68–102, 1997.
 - [97] G. J. Gounaris and F. M. Renard. Specific supersimple properties of $e^- e^+ \rightarrow \gamma H$ at high energy. *Phys. Rev.*, D91(9):093002, 2015.
 - [98] S. Heinemeyer and C. Schappacher. Neutral Higgs boson production at $e^+ e^-$ colliders in the complex MSSM: a full one-loop analysis. *Eur. Phys. J.*, C76(4):220, 2016.
 - [99] Mehmet Demirci. Associated production of Higgs boson with a photon at electron-positron colliders. *Phys. Rev.*, D100:075006, 2019.
 - [100] Abdesslam Arhrib, Rachid Benbrik, and Tzu-Chiang Yuan. Associated Production of Higgs at Linear Collider in the Inert Higgs Doublet Model. *Eur. Phys. J.*, C74:2892, 2014.
 - [101] Shinya Kanemura, Kentarou Mawatari, and Kodai Sakurai. Single Higgs production in association with a photon at electron-positron colliders in extended Higgs models. *Phys. Rev.*, D99(3):035023, 2019.
 - [102] Daruosh Haji Raissi, Seddigheh Tizchang, and Mojtaba Mohammadi Najafabadi. Loop induced singlet scalar production through the vector like top quark at future lepton colliders. *J. Phys. G*, 47(7):075004, 2020.
 - [103] G. J. Gounaris, F. M. Renard, and N. D. Vlachos. Tests of anomalous Higgs boson couplings through $e^- e^+ \rightarrow HZ$ and $H\gamma$. *Nucl. Phys.*, B459:51–74, 1996.
 - [104] Hong-Yu Ren. New Physics Searches with Higgs-photon associated production at the Higgs Factory. *Chin. Phys.*, C39(11):113101, 2015.
 - [105] Qing-Hong Cao, Hao-Ran Wang, and Ya Zhang. Probing $HZ\gamma$ and $H\gamma\gamma$ anomalous couplings in the process $e^+ e^- \rightarrow H\gamma$. *Chin. Phys.*, C39(11):113102, 2015.
 - [106] A. Dedes, K. Suxho, and L. Trifyllis. The decay $h \rightarrow Z\gamma$ in the Standard-Model Effective Field Theory. *JHEP*, 06:115, 2019.

- [107] Gang Li, Hao-Ran Wang, and Shou-hua Zhu. Probing CP-violating $h\bar{t}t$ coupling in $e^+e^- \rightarrow h\gamma$. *Phys. Rev.*, D93(5):055038, 2016.
- [108] Ansgar Denner. Techniques for calculation of electroweak radiative corrections at the one loop level and results for W physics at LEP-200. *Fortsch. Phys.*, 41:307–420, 1993.

APPENDIX

A. PERTURBATIVE UNITARITY ANALYSIS

A.1. Two-fermion process analysis

For the two-fermion process, we take the $t\bar{t} \rightarrow hh$ process as an example. In Fig. 8, we give the



FIG. 8. Feynman diagrams for the $t\bar{t} \rightarrow hh$ scattering process.

Feynman diagrams ⁷. The amplitude with general helicity can be written as

$$\begin{aligned}
 & i\mathcal{M}^{\rho\sigma}(t\bar{t} \rightarrow hh) \\
 &= -i\bar{v}^\sigma(p_2)(y_L^{tT}\omega_- + y_R^{tT}\omega_+)(\frac{1}{\not{p}_1 - \not{k}_1 - m_T} + \frac{1}{\not{p}_1 - \not{k}_2 - m_T})[(y_R^{tT})^*\omega_- + (y_L^{tT})^*\omega_+]u^\rho(p_1) \\
 &= -i\bar{v}^\sigma(p_2)[\frac{m_T(|y_L^{tT}|^2\omega_- + |y_R^{tT}|^2\omega_+) + m_T(y_L^{tT}(y_R^{tT})^*\omega_- + y_R^{tT}(y_L^{tT})^*\omega_+) - (|y_L^{tT}|^2\omega_- + |y_R^{tT}|^2\omega_+)\not{k}_1}{(p_1 - k_1)^2 - m_T^2} \\
 &\quad + \frac{m_T(|y_L^{tT}|^2\omega_- + |y_R^{tT}|^2\omega_+) + m_T(y_L^{tT}(y_R^{tT})^*\omega_- + y_R^{tT}(y_L^{tT})^*\omega_+) - (|y_L^{tT}|^2\omega_- + |y_R^{tT}|^2\omega_+)\not{k}_2}{(p_1 - k_2)^2 - m_T^2}]u^\rho(p_1).
 \end{aligned} \tag{32}$$

In the high energy limit $p_{1,2}^0 \rightarrow \infty$, it can be approximated as

$$i\mathcal{M}^{\rho\sigma}(t\bar{t} \rightarrow hh) \approx i\bar{v}^\sigma(p_2)(|y_L^{tT}|^2\omega_- + |y_R^{tT}|^2\omega_+)[\frac{\not{k}_1}{(p_1 - k_1)^2 - m_T^2} + \frac{\not{k}_2}{(p_1 - k_2)^2 - m_T^2}]u^\rho(p_1). \tag{33}$$

To calculate the above amplitude, we need to choose a reference frame. In the center of mass (COM) frame of initial particles, we can parametrize the momenta p_1, p_2, k_1, k_2 and spinors as follows [41, 108]:

$$\begin{aligned}
 p_1^\mu &= (E_p, 0, 0, |\vec{p}|), & p_2^\mu &= (E_p, 0, 0, -|\vec{p}|), \\
 k_1^\mu &= (E_k, |\vec{k}|\sin\theta, 0, |\vec{k}|\cos\theta), & k_2^\mu &= (E_k, -|\vec{k}|\sin\theta, 0, -|\vec{k}|\cos\theta), \\
 s &= (p_1 + p_2)^2 = (2E_p)^2, & t &= (p_1 - k_1)^2, & u &= (p_1 - k_2)^2,
 \end{aligned}$$

⁷ The diagrams mediated by s -channel Higgs propagator vanish in the high energy limit because of the $\frac{1}{(p_1 + p_2)^2 - m_h^2}$ suppression.

$$\begin{aligned}
u^+(p_1) &= \begin{bmatrix} \sqrt{E_p - |\vec{p}|} \xi^+ \\ \sqrt{E_p + |\vec{p}|} \xi^+ \end{bmatrix}, \quad u^-(p_1) = \begin{bmatrix} \sqrt{E_p + |\vec{p}|} \xi^- \\ \sqrt{E_p - |\vec{p}|} \xi^- \end{bmatrix}, \quad \xi^+ = \begin{bmatrix} 1 \\ 0 \end{bmatrix}, \quad \xi^- = \begin{bmatrix} 0 \\ 1 \end{bmatrix}, \\
v^+(p_2) &= \begin{bmatrix} \sqrt{E_p + |\vec{p}|} \eta^+ \\ -\sqrt{E_p - |\vec{p}|} \eta^+ \end{bmatrix}, \quad v^-(p_2) = \begin{bmatrix} \sqrt{E_p - |\vec{p}|} \eta^- \\ -\sqrt{E_p + |\vec{p}|} \eta^- \end{bmatrix}, \quad \eta^+ = \begin{bmatrix} -1 \\ 0 \end{bmatrix}, \quad \eta^- = \begin{bmatrix} 0 \\ -1 \end{bmatrix}. \quad (34)
\end{aligned}$$

In the high energy limit, we have:

$$\begin{aligned}
p_1^\mu &\approx (E, 0, 0, E), \quad p_2^\mu \approx (E, 0, 0, -E), \\
k_1^\mu &\approx (E, E \sin \theta, 0, E \cos \theta), \quad k_2^\mu \approx (E, -E \sin \theta, 0, -E \cos \theta), \\
s &\approx (2E)^2, \quad t \approx -2E^2(1 - \cos \theta), \quad u \approx -2E^2(1 + \cos \theta).
\end{aligned}$$

$$u^+(p_1) \approx \sqrt{2E} \begin{bmatrix} \vec{0} \\ \xi^+ \end{bmatrix}, \quad u^-(p_1) \approx \sqrt{2E} \begin{bmatrix} \xi^- \\ \vec{0} \end{bmatrix}, \quad v^+(p_2) \approx \sqrt{2E} \begin{bmatrix} \eta^+ \\ \vec{0} \end{bmatrix}, \quad v^-(p_2) \approx \sqrt{2E} \begin{bmatrix} \vec{0} \\ -\eta^- \end{bmatrix}. \quad (35)$$

Thus, we derive the following results:

$$\begin{aligned}
&i\mathcal{M}^{++}(t\bar{t} \rightarrow hh) \\
&\approx -i|y_R^{tT}|^2 \left[\frac{1}{(m_h^2 + m_t^2 - m_T^2)/(2E^2) - (1 - \cos \theta)} - \frac{1}{(m_h^2 + m_t^2 - m_T^2)/(2E^2) - (1 + \cos \theta)} \right], \\
&i\mathcal{M}^{+-}(t\bar{t} \rightarrow hh) \\
&\approx -i|y_L^{tT}|^2 \sin \theta \left[\frac{1}{(m_h^2 + m_t^2 - m_T^2)/(2E^2) - (1 - \cos \theta)} - \frac{1}{(m_h^2 + m_t^2 - m_T^2)/(2E^2) - (1 + \cos \theta)} \right], \\
&i\mathcal{M}^{-+}(t\bar{t} \rightarrow hh) \\
&\approx -i|y_R^{tT}|^2 \sin \theta \left[\frac{1}{(m_h^2 + m_t^2 - m_T^2)/(2E^2) - (1 - \cos \theta)} - \frac{1}{(m_h^2 + m_t^2 - m_T^2)/(2E^2) - (1 + \cos \theta)} \right], \\
&i\mathcal{M}^{--}(t\bar{t} \rightarrow hh) \\
&\approx i|y_L^{tT}|^2 \left[\frac{1}{(m_h^2 + m_t^2 - m_T^2)/(2E^2) - (1 - \cos \theta)} - \frac{1}{(m_h^2 + m_t^2 - m_T^2)/(2E^2) - (1 + \cos \theta)} \right]. \quad (36)
\end{aligned}$$

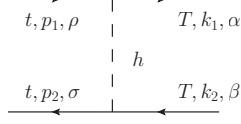
As we can see, there is no S -wave in this channel, namely,

$$a_0^{++}(t\bar{t} \rightarrow hh) \approx a_0^{--}(t\bar{t} \rightarrow hh) \approx a_0^{+-}(t\bar{t} \rightarrow hh) \approx a_0^{-+}(t\bar{t} \rightarrow hh) \approx 0. \quad (37)$$

Of course, there are many other two-fermion processes (for example, $t\bar{T} \rightarrow hh, T\bar{t} \rightarrow hh, T\bar{T} \rightarrow hh, t\bar{t} \rightarrow W^+W^-, t\bar{t} \rightarrow ZZ, t\bar{t} \rightarrow Zh$) depending on the initial and final state particles. Actually, all the two-fermion processes do not contribute to the S -wave [40].

A.2. Four-fermion process analysis

For the four-fermion processes, we take the $t\bar{t} \rightarrow T\bar{T}$ process as an example. In Fig. 9, we give

FIG. 9. Feynman diagram for the $t\bar{t} \rightarrow T\bar{T}$ scattering process.

the Feynman diagram. The amplitude with general helicity can be written as

$$i\mathcal{M}^{\rho\sigma\alpha\beta}(t\bar{t} \rightarrow T\bar{T}) = -\frac{i}{(p_1 - k_1)^2 - m_h^2} \bar{u}^\alpha(k_1)((y_R^{tT})^* \omega_- + (y_L^{tT})^* \omega_+) u^\rho(p_1) \bar{v}^\sigma(p_2)(y_L^{tT} \omega_- + y_R^{tT} \omega_+) v^\beta(k_2). \quad (38)$$

In the COM frame of initial particles, the representations of spinors are listed as follows:

$$\begin{aligned} u^+(p_1) &\approx \sqrt{2E} \begin{bmatrix} \vec{0} \\ \xi^+ \end{bmatrix}, \quad u^-(p_1) \approx \sqrt{2E} \begin{bmatrix} \xi^- \\ \vec{0} \end{bmatrix}, \quad v^+(p_2) \approx \sqrt{2E} \begin{bmatrix} \eta^+ \\ \vec{0} \end{bmatrix}, \quad v^-(p_2) \approx \sqrt{2E} \begin{bmatrix} \vec{0} \\ -\eta^- \end{bmatrix}, \\ u^+(k_1) &\approx \sqrt{2E} \begin{bmatrix} \vec{0} \\ \tilde{\xi}^+ \end{bmatrix}, \quad u^-(k_1) \approx \sqrt{2E} \begin{bmatrix} \tilde{\xi}^- \\ \vec{0} \end{bmatrix}, \quad v^+(k_2) \approx \sqrt{2E} \begin{bmatrix} \tilde{\eta}^+ \\ \vec{0} \end{bmatrix}, \quad v^-(k_2) \approx \sqrt{2E} \begin{bmatrix} \vec{0} \\ -\tilde{\eta}^- \end{bmatrix}, \\ \xi^+ &= \begin{bmatrix} 1 \\ 0 \end{bmatrix}, \quad \xi^- = \begin{bmatrix} 0 \\ 1 \end{bmatrix}, \quad \eta^+ = \begin{bmatrix} -1 \\ 0 \end{bmatrix}, \quad \eta^- = \begin{bmatrix} 0 \\ -1 \end{bmatrix}, \quad \gamma^5 = \begin{bmatrix} -I_{2 \times 2} & 0_{2 \times 2} \\ 0_{2 \times 2} & I_{2 \times 2} \end{bmatrix}, \\ \tilde{\xi}^+ &= \begin{bmatrix} \cos \frac{\theta}{2} \\ \sin \frac{\theta}{2} \end{bmatrix}, \quad \tilde{\xi}^- = \begin{bmatrix} -\sin \frac{\theta}{2} \\ \cos \frac{\theta}{2} \end{bmatrix}, \quad \tilde{\eta}^+ = \begin{bmatrix} -\cos \frac{\theta}{2} \\ -\sin \frac{\theta}{2} \end{bmatrix}, \quad \tilde{\eta}^- = \begin{bmatrix} \sin \frac{\theta}{2} \\ -\cos \frac{\theta}{2} \end{bmatrix}. \end{aligned} \quad (39)$$

Then, we can get the polarized amplitudes:

$$\begin{aligned} i\mathcal{M}^{++++}(t\bar{t} \rightarrow T\bar{T}) &\approx i\mathcal{M}^{+++-}(t\bar{t} \rightarrow T\bar{T}) \approx i\mathcal{M}^{++-+}(t\bar{t} \rightarrow T\bar{T}) \approx 0, \\ i\mathcal{M}^{++--}(t\bar{t} \rightarrow T\bar{T}) &\approx \frac{is y_R^{tT} (y_L^{tT})^* \sin^2 \frac{\theta}{2}}{(p_1 - k_1)^2 - m_h^2}, \\ i\mathcal{M}^{+-++}(t\bar{t} \rightarrow T\bar{T}) &\approx i\mathcal{M}^{+--+}(t\bar{t} \rightarrow T\bar{T}) \approx i\mathcal{M}^{+---}(t\bar{t} \rightarrow T\bar{T}) \approx 0, \\ i\mathcal{M}^{+--+}(t\bar{t} \rightarrow T\bar{T}) &\approx -\frac{is |y_L^{tT}|^2 \sin^2 \frac{\theta}{2}}{(p_1 - k_1)^2 - m_h^2}, \\ i\mathcal{M}^{-+++}(t\bar{t} \rightarrow T\bar{T}) &\approx i\mathcal{M}^{-++-}(t\bar{t} \rightarrow T\bar{T}) \approx i\mathcal{M}^{-+-+}(t\bar{t} \rightarrow T\bar{T}) \approx 0, \\ i\mathcal{M}^{-++-}(t\bar{t} \rightarrow T\bar{T}) &\approx -\frac{is |y_R^{tT}|^2 \sin^2 \frac{\theta}{2}}{(p_1 - k_1)^2 - m_h^2}, \\ i\mathcal{M}^{--++}(t\bar{t} \rightarrow T\bar{T}) &\approx \frac{is y_L^{tT} (y_R^{tT})^* \sin^2 \frac{\theta}{2}}{(p_1 - k_1)^2 - m_h^2}, \\ i\mathcal{M}^{--+-}(t\bar{t} \rightarrow T\bar{T}) &\approx i\mathcal{M}^{---+}(t\bar{t} \rightarrow T\bar{T}) \approx i\mathcal{M}^{----}(t\bar{t} \rightarrow T\bar{T}) \approx 0. \end{aligned} \quad (40)$$

In general, the initial and final states both can be $t\bar{t}, t\bar{T}, T\bar{t}, T\bar{T}$. Thus, the coupled channel matrix is 16×16 (four states plus four helicity cases) even if we do not consider the color degrees of

freedom. To make the problem as simple as possible, we only turn on the y_L^{tT}, y_R^{tT} couplings. Under this consideration, the non-zero coupled channel amplitudes are

$$\begin{aligned}\mathcal{M}^{++--}(t\bar{t} \rightarrow T\bar{T}) &\approx \frac{sy_R^{tT}(y_L^{tT})^* \sin^2 \frac{\theta}{2}}{(p_1 - k_1)^2 - m_h^2}, & \mathcal{M}^{+--+}(t\bar{t} \rightarrow T\bar{T}) &\approx -\frac{s|y_L^{tT}|^2 \sin^2 \frac{\theta}{2}}{(p_1 - k_1)^2 - m_h^2}, \\ \mathcal{M}^{-++-}(t\bar{t} \rightarrow T\bar{T}) &\approx -\frac{s|y_R^{tT}|^2 \sin^2 \frac{\theta}{2}}{(p_1 - k_1)^2 - m_h^2}, & \mathcal{M}^{--++}(t\bar{t} \rightarrow T\bar{T}) &\approx \frac{sy_L^{tT}(y_R^{tT})^* \sin^2 \frac{\theta}{2}}{(p_1 - k_1)^2 - m_h^2}.\end{aligned}\quad (41)$$

The corresponding S -wave amplitudes are calculated to be

$$\begin{aligned}a_0^{++--}(t\bar{t} \rightarrow T\bar{T}) &\approx -\frac{y_R^{tT}(y_L^{tT})^*}{16\pi}, & a_0^{+--+}(t\bar{t} \rightarrow T\bar{T}) &\approx \frac{|y_L^{tT}|^2}{16\pi}, \\ a_0^{-++-}(t\bar{t} \rightarrow T\bar{T}) &\approx \frac{|y_R^{tT}|^2}{16\pi}, & a_0^{--++}(t\bar{t} \rightarrow T\bar{T}) &\approx -\frac{y_L^{tT}(y_R^{tT})^*}{16\pi}.\end{aligned}\quad (42)$$

In the basis of $++$, $+-$, $-+$, $--$, we can get the following coupled channel matrix for this process:

$$a_0(t\bar{t} \rightarrow T\bar{T}) = \frac{1}{16\pi} \begin{bmatrix} 0 & 0 & 0 & -y_R^{tT}(y_L^{tT})^* \\ 0 & 0 & |y_L^{tT}|^2 & 0 \\ 0 & |y_R^{tT}|^2 & 0 & 0 \\ -y_L^{tT}(y_R^{tT})^* & 0 & 0 & 0 \end{bmatrix}. \quad (43)$$

Similarly, we can get the following coupled channel matrices for the other processes in the basis of $++$, $+-$, $-+$, $--$:

$$a_0(T\bar{T} \rightarrow t\bar{t}) = \frac{1}{16\pi} \begin{bmatrix} 0 & 0 & 0 & -y_R^{tT}(y_L^{tT})^* \\ 0 & 0 & |y_L^{tT}|^2 & 0 \\ 0 & |y_R^{tT}|^2 & 0 & 0 \\ -y_L^{tT}(y_R^{tT})^* & 0 & 0 & 0 \end{bmatrix}, \quad (44)$$

$$a_0(t\bar{T} \rightarrow t\bar{T}) = \frac{1}{16\pi} \begin{bmatrix} -|y_L^{tT}|^2 & 0 & 0 & y_R^{tT}(y_L^{tT})^* \\ 0 & 0 & 0 & 0 \\ 0 & 0 & 0 & 0 \\ y_L^{tT}(y_R^{tT})^* & 0 & 0 & -|y_R^{tT}|^2 \end{bmatrix}, \quad (45)$$

$$a_0(t\bar{T} \rightarrow T\bar{t}) = \frac{1}{16\pi} \begin{bmatrix} -(y_L^{tT})^*(y_R^{tT})^* & 0 & 0 & 0 \\ 0 & 0 & (y_L^{tT})^*(y_R^{tT})^* & 0 \\ 0 & (y_L^{tT})^*(y_R^{tT})^* & 0 & 0 \\ 0 & 0 & 0 & -(y_L^{tT})^*(y_R^{tT})^* \end{bmatrix}, \quad (46)$$

$$a_0(T\bar{t} \rightarrow t\bar{T}) = \frac{1}{16\pi} \begin{bmatrix} -y_L^{tT}y_R^{tT} & 0 & 0 & 0 \\ 0 & 0 & y_L^{tT}y_R^{tT} & 0 \\ 0 & y_L^{tT}y_R^{tT} & 0 & 0 \\ 0 & 0 & 0 & -y_L^{tT}y_R^{tT} \end{bmatrix}, \quad (47)$$

$$a_0(T\bar{t} \rightarrow T\bar{t}) = \frac{1}{16\pi} \begin{bmatrix} -|y_R^{tT}|^2 & 0 & 0 & y_R^{tT}(y_L^{tT})^* \\ 0 & 0 & 0 & 0 \\ 0 & 0 & 0 & 0 \\ y_L^{tT}(y_R^{tT})^* & 0 & 0 & -|y_L^{tT}|^2 \end{bmatrix}. \quad (48)$$

In the basis of $t\bar{t}, T\bar{T}, t\bar{T}, T\bar{t}$, we can get the following coupled channel matrix for all the four-fermion processes without regard to the quark color:

$$a_0 = \begin{bmatrix} 0_{4 \times 4} & a_0(t\bar{t} \rightarrow T\bar{T}) & 0_{4 \times 4} & 0_{4 \times 4} \\ a_0(T\bar{T} \rightarrow t\bar{t}) & 0_{4 \times 4} & 0_{4 \times 4} & 0_{4 \times 4} \\ 0_{4 \times 4} & 0_{4 \times 4} & a_0(t\bar{T} \rightarrow t\bar{T}) & a_0(t\bar{T} \rightarrow T\bar{t}) \\ 0_{4 \times 4} & 0_{4 \times 4} & a_0(T\bar{t} \rightarrow t\bar{T}) & a_0(T\bar{t} \rightarrow T\bar{t}) \end{bmatrix}. \quad (49)$$

In the above, we write the coupled channel matrix in the block form. Obviously, this square matrix is 16×16 . Then we can get the eigenvalues of a_0 as follows ⁸:

$$\begin{aligned} \lambda_1^+ &= \frac{1}{16\pi} |y_L^{tT}|^2, & \lambda_1^- &= -\frac{1}{16\pi} |y_L^{tT}|^2, & \lambda_2^+ &= \frac{1}{16\pi} |y_R^{tT}|^2, & \lambda_2^- &= -\frac{1}{16\pi} |y_R^{tT}|^2, \\ \lambda_3^+ &= \frac{1}{16\pi} |y_L^{tT}| |y_R^{tT}|, & \lambda_3^- &= -\frac{1}{16\pi} |y_L^{tT}| |y_R^{tT}|, \\ \lambda_4^+ &= \frac{1}{32\pi} (\sqrt{(|y_L^{tT}|^2 + |y_R^{tT}|^2)^2 + 12|y_L^{tT}|^2 |y_R^{tT}|^2} - |y_L^{tT}|^2 - |y_R^{tT}|^2), \\ \lambda_4^- &= \frac{1}{32\pi} (-\sqrt{(|y_L^{tT}|^2 + |y_R^{tT}|^2)^2 + 12|y_L^{tT}|^2 |y_R^{tT}|^2} - |y_L^{tT}|^2 - |y_R^{tT}|^2), \end{aligned} \quad (50)$$

where λ_1^-, λ_2^- are doubly degenerate and λ_3^+, λ_3^- are four-fold degenerate. S -wave unitarity requires that all the eigenvalues must satisfy $|\text{Re}(\lambda_i)| \leq \frac{1}{2}$. It will lead to the following constraints ⁹:

$$\sqrt{(|y_L^{tT}|^2 + |y_R^{tT}|^2)^2 + 12|y_L^{tT}|^2 |y_R^{tT}|^2} + |y_L^{tT}|^2 + |y_R^{tT}|^2 \leq 16\pi. \quad (51)$$

Note that $|y_L^{tT}| \leq \sqrt{8\pi}, |y_R^{tT}| \leq \sqrt{8\pi}, \sqrt{|y_L^{tT}| |y_R^{tT}|} \leq \sqrt{8\pi}$ hold automatically in the above bound.

B. $h \rightarrow \gamma\gamma$ CHANNEL ANALYSIS

B.1. SM result

The partial decay width of $h \rightarrow \gamma\gamma$ for SM is given in Refs. [69, 71]

$$\Gamma^{SM}(h \rightarrow \gamma\gamma) = \frac{G_F \alpha^2 m_h^3}{128 \sqrt{2} \pi^3} \left| \sum_f N_f^C Q_f^2 F_f(\tau_f) + F_W(\tau_W) \right|^2 \left(\tau_f = \frac{4m_f^2}{m_h^2}, \tau_W = \frac{4m_W^2}{m_h^2} \right), \quad (52)$$

⁸ When we take the quark color into account further, the matrix will become 48×48 . Although the unitarity bounds may be improved, the matrix will be quite large and complex to deal with.

⁹ Remember that the bounds are just a rough estimation. If we turn on the other couplings (say y_T, κ_t), these constraints may be altered.

with the F_f, F_W defined by

$$F_f(\tau_f) \equiv -2\tau_f[1 + (1 - \tau_f)f(\tau_f)], \quad F_W(\tau_W) \equiv 2 + 3\tau_W + 3\tau_W(2 - \tau_W)f(\tau_W),$$

$$f(\tau) \equiv \begin{cases} \arcsin^2(\frac{1}{\sqrt{\tau}}), & \text{for } \tau \geq 1 \\ -\frac{1}{4}[\log \frac{1+\sqrt{1-\tau}}{1-\sqrt{1-\tau}} - i\pi]^2, & \text{for } \tau < 1 \end{cases}. \quad (53)$$

For the fermionic part, the top quark is dominated because of the largest Yukawa coupling. Numerically, we can get $N_t^C Q_t^2 F_f(\tau_t) \sim -1.84$, $F_W(\tau_W) \sim 8.32$. This means the gauge boson contributions are almost 4.5 times larger than the fermionic ones.

B.2. New physics result

Due to $U_{EM}(1)$ gauge symmetry, the $h \rightarrow \gamma\gamma$ amplitude possesses the following tensor structure:

$$i\mathcal{M} = i\epsilon_\mu(p_1)\epsilon_\nu(p_2)(p_2^\mu p_1^\nu - p_1 \cdot p_2 g^{\mu\nu})\mathcal{A}^\gamma, \quad \mathcal{A}^\gamma \equiv \frac{e^2}{8\pi^2 v}(-F_W(\tau_W) + \mathcal{A}_t^\gamma + \mathcal{A}_T^\gamma). \quad (54)$$

The expressions of $\mathcal{A}_t^\gamma, \mathcal{A}_T^\gamma$ are given as

$$\mathcal{A}_t^\gamma = -N_t^C Q_t^2 \kappa_t F_f(\tau_t), \quad \mathcal{A}_T^\gamma = N_T^C Q_T^2 \frac{y_T v}{m_T} F_f(\tau_T). \quad (55)$$

Taking the mass of t, T quarks to be infinity, they can be expanded as

$$\mathcal{A}_t^\gamma \approx -N_t^C Q_t^2 \kappa_t (-\frac{4}{3} - \frac{7m_h^2}{90m_t^2}), \quad \mathcal{A}_T^\gamma \approx N_T^C Q_T^2 \frac{y_T v}{m_T} (-\frac{4}{3} - \frac{7m_h^2}{90m_T^2}),$$

$$\mathcal{A}_t^\gamma + \mathcal{A}_T^\gamma \approx \frac{4}{3} N_t^C Q_t^2 [(\kappa_t - \frac{y_T v}{m_T}) + \kappa_t \cdot \frac{7m_h^2}{120m_t^2} - \frac{y_T v}{m_T} \cdot \frac{7m_h^2}{120m_T^2}]. \quad (56)$$

The partial decay width formula is computed as ¹⁰:

$$\Gamma(h \rightarrow \gamma\gamma) = \frac{G_F \alpha^2 m_h^3}{128\sqrt{2}\pi^3} |A_t^\gamma + A_T^\gamma - F_W(\tau_W)|^2 = \frac{G_F \alpha^2 m_h^3}{128\sqrt{2}\pi^3} |N_t^C Q_t^2 [\kappa_t F_f(\tau_t) - \frac{y_T v}{m_T} F_f(\tau_T)] + F_W(\tau_W)|^2. \quad (57)$$

In Tab. IV, we list the expressions of $A_t^\gamma + A_T^\gamma$ in several models, where we have neglected the $\frac{1}{m_{t,T}^4}$ suppressed terms. We can see that the $A_t^\gamma + A_T^\gamma$ in VLQT and VLQT+S models are close to those in SM. In fact, it is difficult to detect VLQ in the $h\gamma\gamma$ decay channel [21].

¹⁰ The $h \rightarrow gg$ partial decay width is similar to the fermionic part of the $\gamma\gamma$ decay.

	$\bar{A}_t^\gamma + \bar{A}_T^\gamma$
General	$\frac{4}{3}[(\kappa_t - \frac{y_T v}{m_T}) + \kappa_t \cdot \frac{7m_h^2}{120m_t^2} - \frac{y_T v}{m_T} \cdot \frac{7m_h^2}{120m_T^2}]$
SM	$\frac{4}{3}(1 + \frac{7m_h^2}{120m_t^2})$
VLQT	$\frac{4}{3}(1 + c_L^2 \cdot \frac{7m_h^2}{120m_t^2} + s_L^2 \cdot \frac{7m_h^2}{120m_T^2})$
VLQT+S	$\frac{4}{3}[c_\theta - \frac{v}{m_T} \text{Re}(y_T^S) s_\theta \frac{c_R}{c_L} + (c_L^2 c_\theta - \frac{v}{m_T} \text{Re}(y_T^S) s_\theta \frac{s_L^2 c_R}{c_L}) \cdot \frac{7m_h^2}{120m_t^2} + (s_L^2 c_\theta - \frac{v}{m_T} \text{Re}(y_T^S) s_\theta c_L c_R) \cdot \frac{7m_h^2}{120m_T^2}]$

TABLE IV. The expressions of $\bar{A}_t^\gamma + \bar{A}_T^\gamma$ in the SM, VLQT, and VLQT+S under the heavy quark limit. Here, we extract the common factor $N_t^C Q_t^2$ for convenience, that is, redefinition of A^γ with $N_t^C Q_t^2 \bar{A}^\gamma$. We take $\bar{A}_T^\gamma = 0$ naively in the SM because of the absence of a T quark.

C. ASYMPTOTIC BEHAVIORS OF THE LOOP FUNCTIONS

The B_0 function is defined as [108]

$$\begin{aligned}
& B_0(k^2, m_0^2, m_1^2) \\
& \equiv \frac{(2\pi\mu)^{4-D}}{i\pi^2} \int d^D q \frac{1}{(q^2 - m_0^2)[(q+k)^2 - m_1^2]} \\
& = \Delta_\epsilon - \int_0^1 dx \log \frac{xm_1^2 + (1-x)m_0^2 - x(1-x)k^2}{\mu^2} \quad (\Delta_\epsilon = \frac{1}{\epsilon} - \gamma_E + \log 4\pi, \quad D = 4 - 2\epsilon). \quad (58)
\end{aligned}$$

In the limit of $k^2 \ll m_0^2, m_1^2$, the B_0 function can be expanded as

$$\begin{aligned}
& B_0(k^2, m_0^2, m_1^2) \\
& = B_0(0, m_0^2, m_1^2) + \frac{\partial B_0(k^2, m_0^2, m_1^2)}{\partial k^2} \Big|_{k^2=0} k^2 + \mathcal{O}(\frac{k^4}{m_0^4}, \frac{k^4}{m_0^2 m_1^2}, \frac{k^4}{m_1^4}) \\
& = \Delta_\epsilon + 1 - \frac{m_0^2 \log \frac{m_0^2}{\mu^2} - m_1^2 \log \frac{m_1^2}{\mu^2}}{m_0^2 - m_1^2} + \frac{m_0^4 - m_1^4 + 2m_0^2 m_1^2 \log \frac{m_1^2}{m_0^2}}{2(m_0^2 - m_1^2)^3} k^2 + \mathcal{O}(\frac{k^4}{m_0^4}, \frac{k^4}{m_0^2 m_1^2}, \frac{k^4}{m_1^4}). \quad (59)
\end{aligned}$$

The C_0 function is defined as

$$\begin{aligned}
& C_0(k_1^2, k_{12}^2, k_2^2, m_0^2, m_1^2, m_2^2) \quad (k_{12} \equiv k_1 - k_2) \\
& \equiv \frac{(2\pi\mu)^{4-D}}{i\pi^2} \int d^D q \frac{1}{(q^2 - m_0^2)[(q+k_1)^2 - m_1^2][(q+k_2)^2 - m_2^2]} \\
& = - \int_0^1 \int_0^1 \int_0^1 dx dy dz \frac{\delta(x+y+z-1)}{(yk_1 + zk_2)^2 + xm_0^2 + ym_1^2 + zm_2^2 - yk_1^2 - zk_2^2}. \quad (60)
\end{aligned}$$

Then, we have

$$\begin{aligned}
C_0(0, m_Z^2, m_h^2, m_t^2, m_T^2) &= C_0(0, m_Z^2, m_h^2, m_T^2, m_t^2) \\
&= - \int_0^1 \int_0^1 \int_0^1 dx dy dz \frac{\delta(x+y+z-1)}{[yp_1 + z(p_1 + p_2)]^2 + (x+y)m_t^2 + zm_T^2 - yp_1^2 - z(p_1 + p_2)^2} \\
&= - \int_0^1 \int_0^1 \int_0^1 dx dy dz \frac{\delta(x+y+z-1)}{yz(m_h^2 - m_Z^2) + z^2 m_h^2 + (x+y)m_t^2 + zm_T^2 - zm_h^2}.
\end{aligned} \tag{61}$$

In the limit of $m_h, m_Z \ll m_f$, the $C_0(0, m_Z^2, m_h^2, m_f^2, m_f^2)$ function can be expanded as

$$C_0(0, m_Z^2, m_h^2, m_f^2, m_f^2) = -\frac{1}{2m_f^2} \left[1 + \frac{m_h^2 + m_Z^2}{12m_f^2} + \mathcal{O}\left(\frac{m_h^4, m_h^2 m_Z^2, m_Z^4}{m_f^4}\right) \right]. \tag{62}$$

In the limit of $m_h, m_Z \ll m_t, m_T$, the $C_0(0, m_Z^2, m_h^2, m_t^2, m_T^2)$ function can be expanded as

$$\begin{aligned}
C_0(0, m_Z^2, m_h^2, m_t^2, m_T^2) &= C_0(0, 0, 0, m_t^2, m_T^2) + \frac{\partial C_0(0, m_Z^2, m_h^2, m_t^2, m_T^2)}{\partial m_h^2} \Big|_{(m_h=0, m_Z=0)} m_h^2 \\
&+ \frac{\partial C_0(0, m_Z^2, m_h^2, m_t^2, m_T^2)}{\partial m_Z^2} \Big|_{(m_h=0, m_Z=0)} m_Z^2 + \mathcal{O}\left(\frac{m_h^4, m_h^2 m_Z^2, m_Z^4}{m_t^6, m_t^4 m_T^2, m_t^2 m_T^4, m_T^6}\right),
\end{aligned} \tag{63}$$

with

$$\begin{aligned}
C_0(0, 0, 0, m_t^2, m_T^2) &= C_0(0, 0, 0, m_T^2, m_t^2) = \frac{1}{m_T^2} \frac{1 - r_{tT}^2 + \log r_{tT}^2}{(1 - r_{tT}^2)^2} \quad (r_{tT} = \frac{m_t}{m_T}), \\
\frac{\partial C_0(0, m_Z^2, m_h^2, m_t^2, m_T^2)}{\partial m_h^2} \Big|_{(m_h=0, m_Z=0)} &= \frac{\partial C_0(0, m_Z^2, m_h^2, m_t^2, m_T^2)}{\partial m_Z^2} \Big|_{(m_h=0, m_Z=0)} \\
&= \frac{1}{m_T^4} \frac{2(1 + 2r_{tT}^2) \log r_{tT}^2 + 5 - 4r_{tT}^2 - r_{tT}^4}{4(1 - r_{tT}^2)^4}.
\end{aligned} \tag{64}$$

Thus, we have

$$C_0(0, m_Z^2, m_h^2, m_t^2, m_T^2) \approx \frac{1}{m_T^2} \left[1 + \log r_{tT}^2 + \frac{m_h^2 + m_Z^2}{m_T^2} \frac{5 + 2(1 + 2r_{tT}^2) \log r_{tT}^2}{4} \right]. \tag{65}$$

For the case of $C_0(0, m_Z^2, m_h^2, m_T^2, m_t^2)$, we can get the corresponding results via the replacement $m_t \leftrightarrow m_T$. For example, we have

$$C_0(0, m_Z^2, m_h^2, m_T^2, m_t^2) \approx -\frac{1}{m_T^2} \left[1 + r_{tT}^2 \log r_{tT}^2 + \frac{m_h^2 + m_Z^2}{m_T^2} \frac{1 + 4r_{tT}^2 \log r_{tT}^2}{4} \right]. \tag{66}$$

Here, we also give the heavy m_f expansion of the following functions:

$$f(\tau_f) = \frac{m_h^2}{4m_f^2} + \frac{m_h^4}{48m_f^4} + \mathcal{O}\left(\frac{m_h^6}{m_f^6}\right), \quad F_f(\tau_f) = -\frac{4}{3} - \frac{7m_h^2}{90m_f^2} + \mathcal{O}\left(\frac{m_h^4}{m_f^4}\right). \tag{67}$$

and

$$\begin{aligned}
A_f(\tau_f, \lambda_f) &= \frac{m_f^2}{m_h^2 - m_Z^2} [(m_h^2 - m_Z^2 - 4m_f^2)C_0(0, m_Z^2, m_h^2, m_f^2, m_f^2, m_f^2) - 2m_Z^2 \frac{B_0(m_h^2, m_f^2, m_f^2) - B_0(m_Z^2, m_f^2, m_f^2)}{m_h^2 - m_Z^2} - 2] \\
&= -\frac{1}{3} - \frac{7m_h^2 + 11m_Z^2}{360m_f^2} + \mathcal{O}\left(\frac{m_h^4, m_h^2 m_Z^2, m_Z^4}{m_f^4}\right).
\end{aligned} \tag{68}$$

In the following, we list some special limits of the loop integrals:

$$\begin{aligned}
\lim_{\tau_f \rightarrow 0} F_f(\tau_f) &= 0, \quad \lim_{\tau_f \rightarrow \infty} F_f(\tau_f) = -\frac{4}{3}, \\
\lim_{\tau_W \rightarrow 0} F_W(\tau_W) &= 2, \quad \lim_{\tau_W \rightarrow \infty} F_W(\tau_W) = 7, \\
\lim_{\lambda \rightarrow \infty} I_1(\tau, \lambda) &= \frac{\tau^2}{2} f(\tau) - \frac{\tau}{2}, \quad \lim_{\lambda \rightarrow \infty} I_2(\tau, \lambda) = \frac{\tau}{2} f(\tau), \\
\lim_{\lambda_f \rightarrow \infty} A_f(\tau_f, \lambda_f) &= \frac{\tau_f}{2} [(\tau_f - 1)f(\tau_f) - 1] = \frac{1}{4} F_f(\tau_f), \\
\lim_{\lambda_W \rightarrow \infty} A_W(\tau_W, \lambda_W) &= \frac{1}{2t_W} [(5 - t_W^2)\tau_W(2 - \tau_W)f(\tau_W) + 2 + 5\tau_W - t_W^2(2 + \tau_W)].
\end{aligned} \tag{69}$$